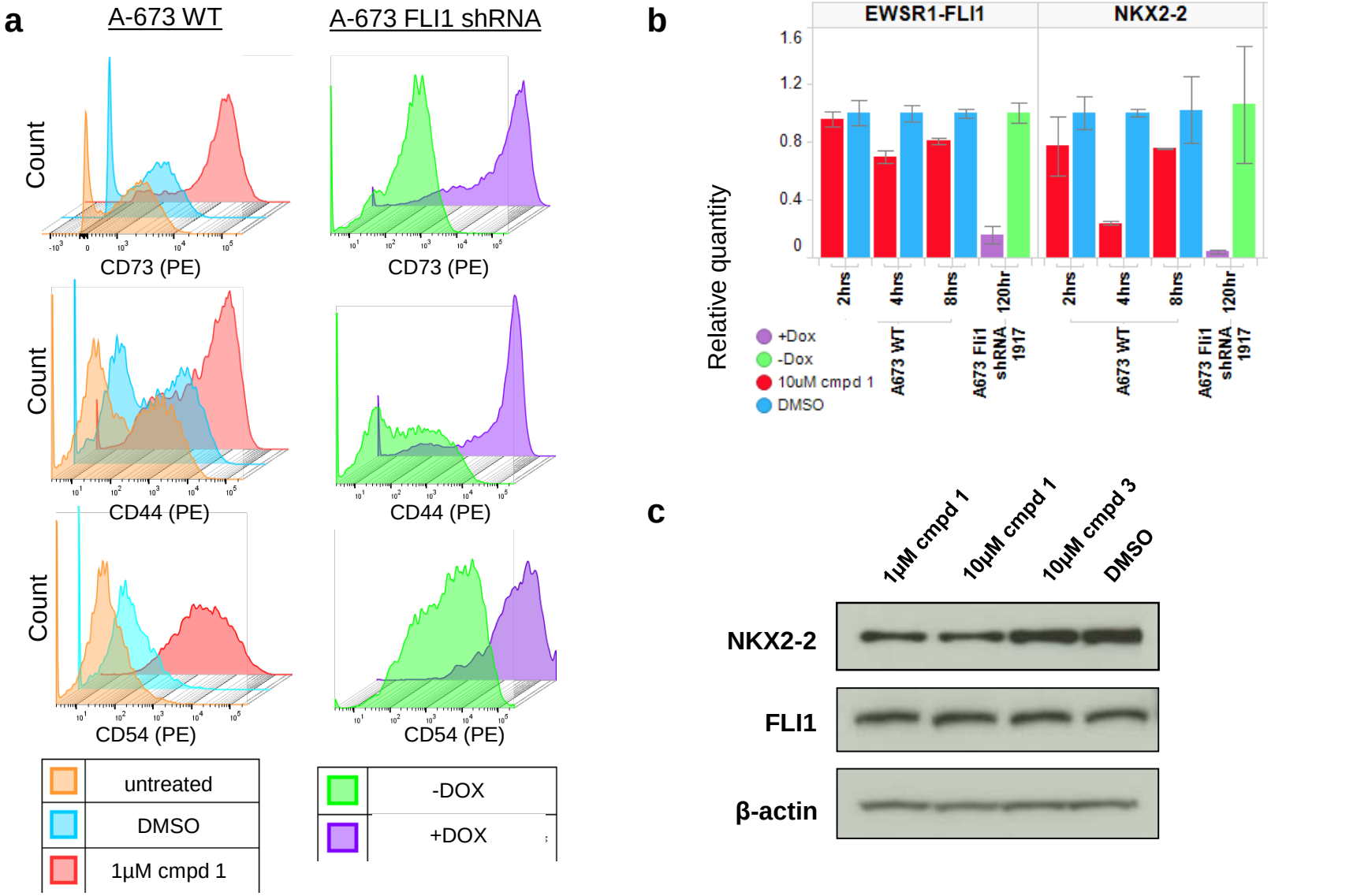

Supplementary Figure 1: **a**, FACS read-out for cell surface differentiation markers in A-673 cells, following compound **1** treatment (left panels) or upon knock-down of EWS-FLI in A-673 cells stably transduced with a vector containing published shRNA 1917 against FLI1 (right panels) (n=2). **b**,**c**, Analysis of EWS-FLI1 target gene NKX2-2 expression in response to treatment of A-673 cells with compound 1 by (**b**) RT-qPCR, with doxycycline (dox) inducible shRNA-mediated knock-down of EWS-FLI1 for comparison (relative quantification by standard curve was applied for all qPCR reactions, normalizing transcript quantities per target gene to those of endogenous control PPIA per sample and setting the DMSO-treated condition per target gene equal to 1. Center represents mean and error bars represent standard deviation, with three biological replicates per condition), or (**c**) by western blot with β-actin as loading control (repeated two independent times).

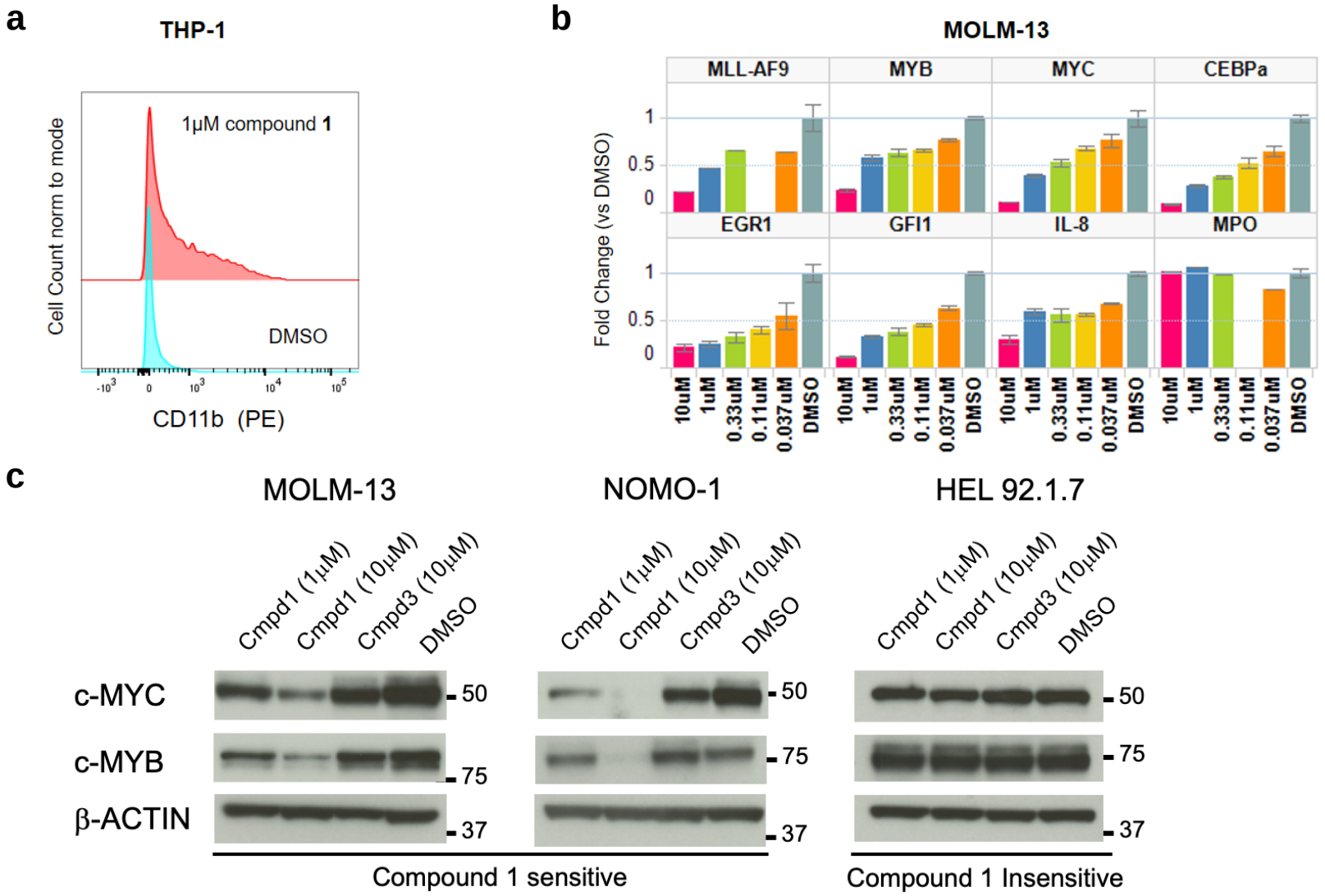

Supplementary Figure 2: **a**, FACS read-out for cell surface differentiation marker CD11b in THP-1 cells following compound **1** treatment for 72 h (n=1). **b**, Expression analysis by RT-qPCR of MLL-AF9 and a panel of known target genes in MOLM-13 cells treated with compound **1** in dose-response for 4 h (relative quantification by standard curve was applied for all qPCR reactions, normalizing transcript quantities per target gene to those of endogenous control PPIA per sample and setting the DMSO-treated condition per target gene equal to 1. Center value represents mean, error bars represent standard deviation, with three biological replicates, except for MLL-AF9 and MPO, which were processed as three technical replicates of one biological replicate). **c**, Expression analysis by western blot of c-MYC and c-MYB in response to compound **1** treatment comparing compound-sensitive AML cell lines with MLL-fusion (MOLM-13 and NOMO-1) to compound-insensitive and non-translocated AML cell line HEL 92.1.7 (repeated 3 independent times). An uncropped scan of this blot is provided in Supplementary Figure 20.

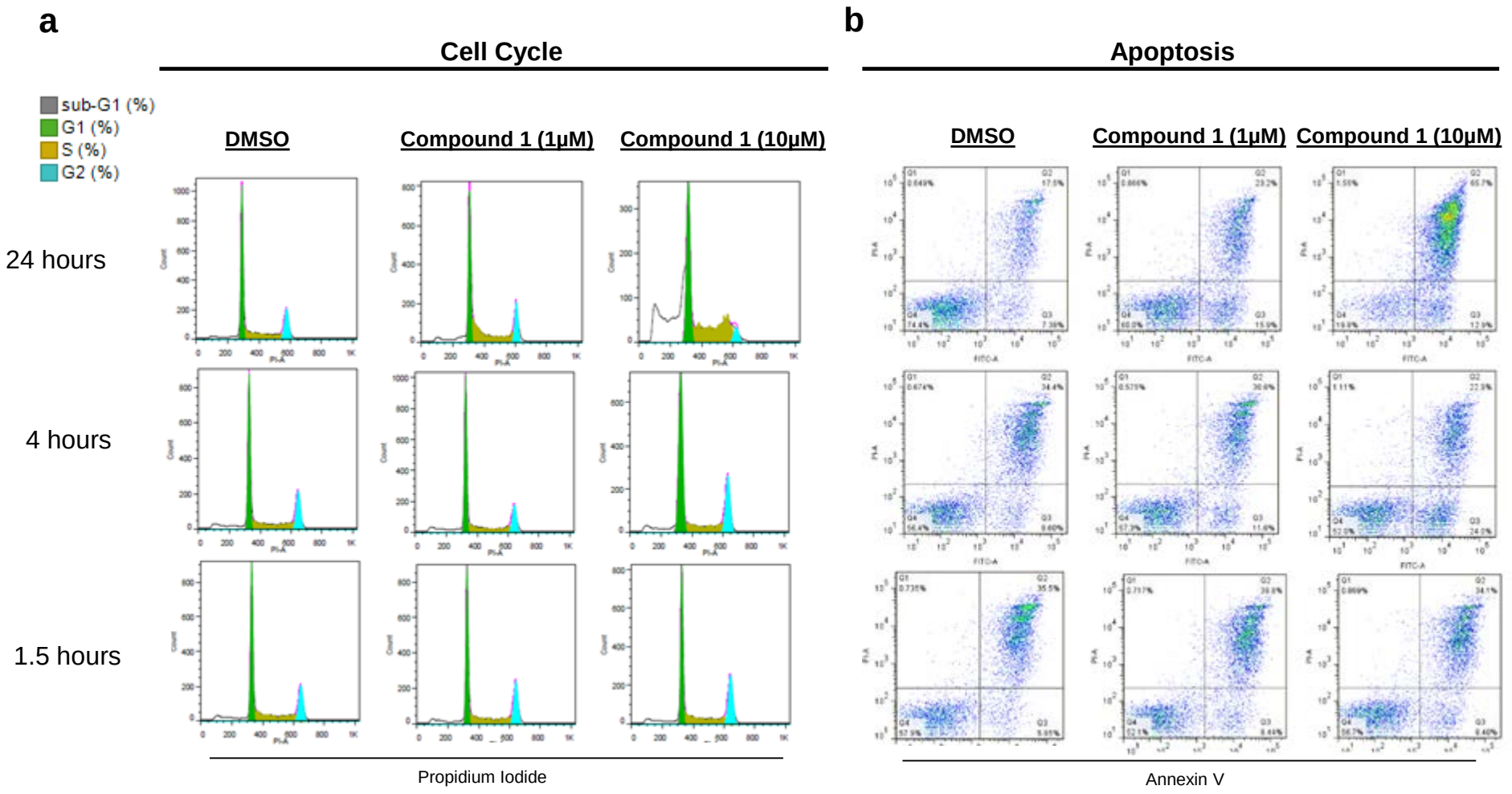

Supplementary Figure 3: **a**, Cell cycle analysis by propidium iodine staining or **b**, apoptosis assessment by Annexin V staining and FACS read-out in NOMO-1 cells treated with compound **1** as indicated (repeated independently two times).

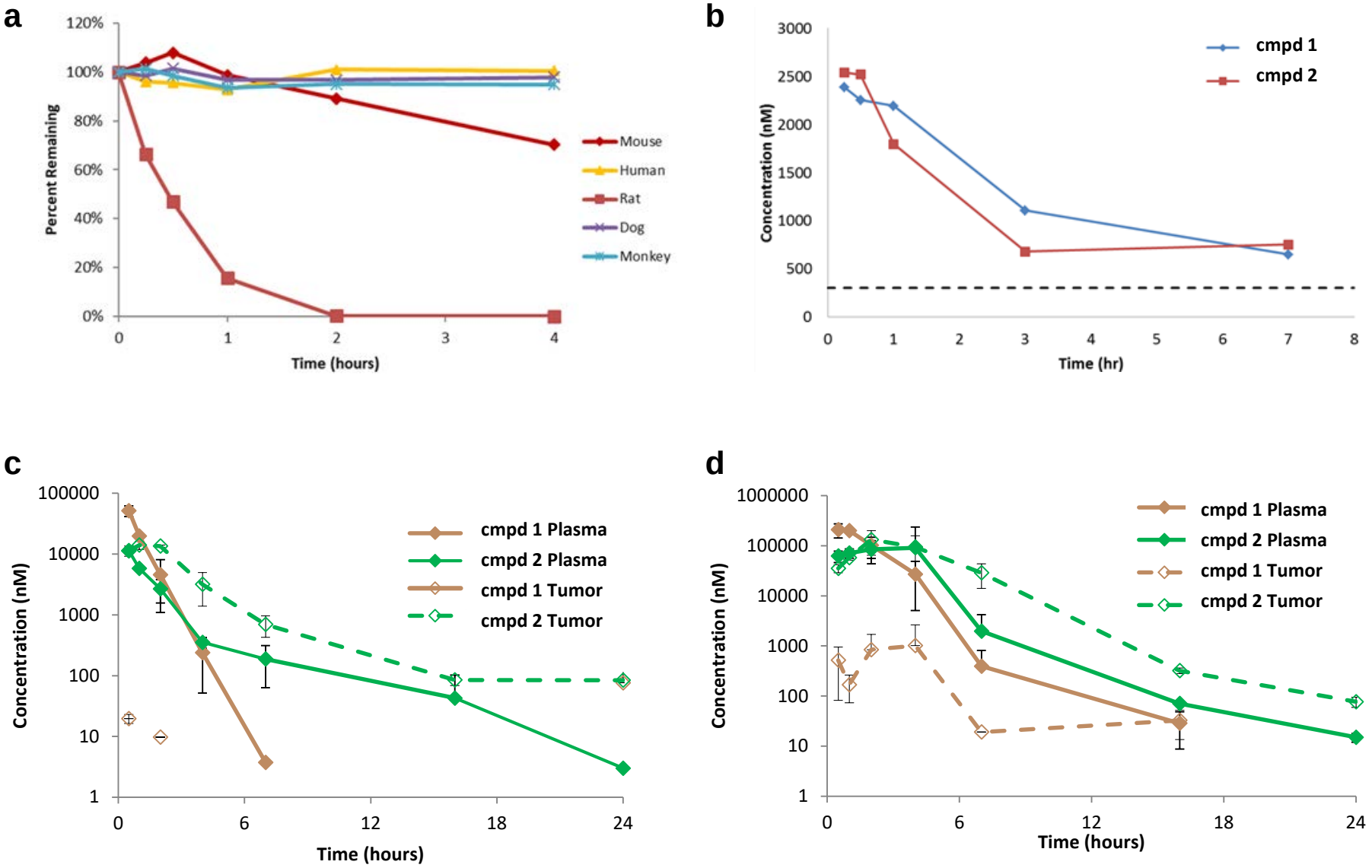

Supplementary Figure 4: MOLM-13 xenograft mouse *in vivo* study, including plasma stability and pharmacokinetics. **a**, Assessment of compound **1** stability in plasma per species as indicated, incubating 2.5µg/ml of **1** at 37°C for 4.5h in presence of K2 EDTA as anti-coagulant. **b**, Plasma concentration over time of compound **1** and **2** when dosing **1** subcutaneously in mice at 30mg/kg (n = 2). Black dashed line represents compound **1** IC_{50} value in MOLM-13 cell line. **c**,**d**, Plasma and tumor concentration over time of compound **1** and **2** when dosing **1** subcutaneously at (**c**) 100 mg/kg or (**d**) at 400 mg/kg in mouse xenograft model (n = 3, presented as mean plus/minus standard deviation).

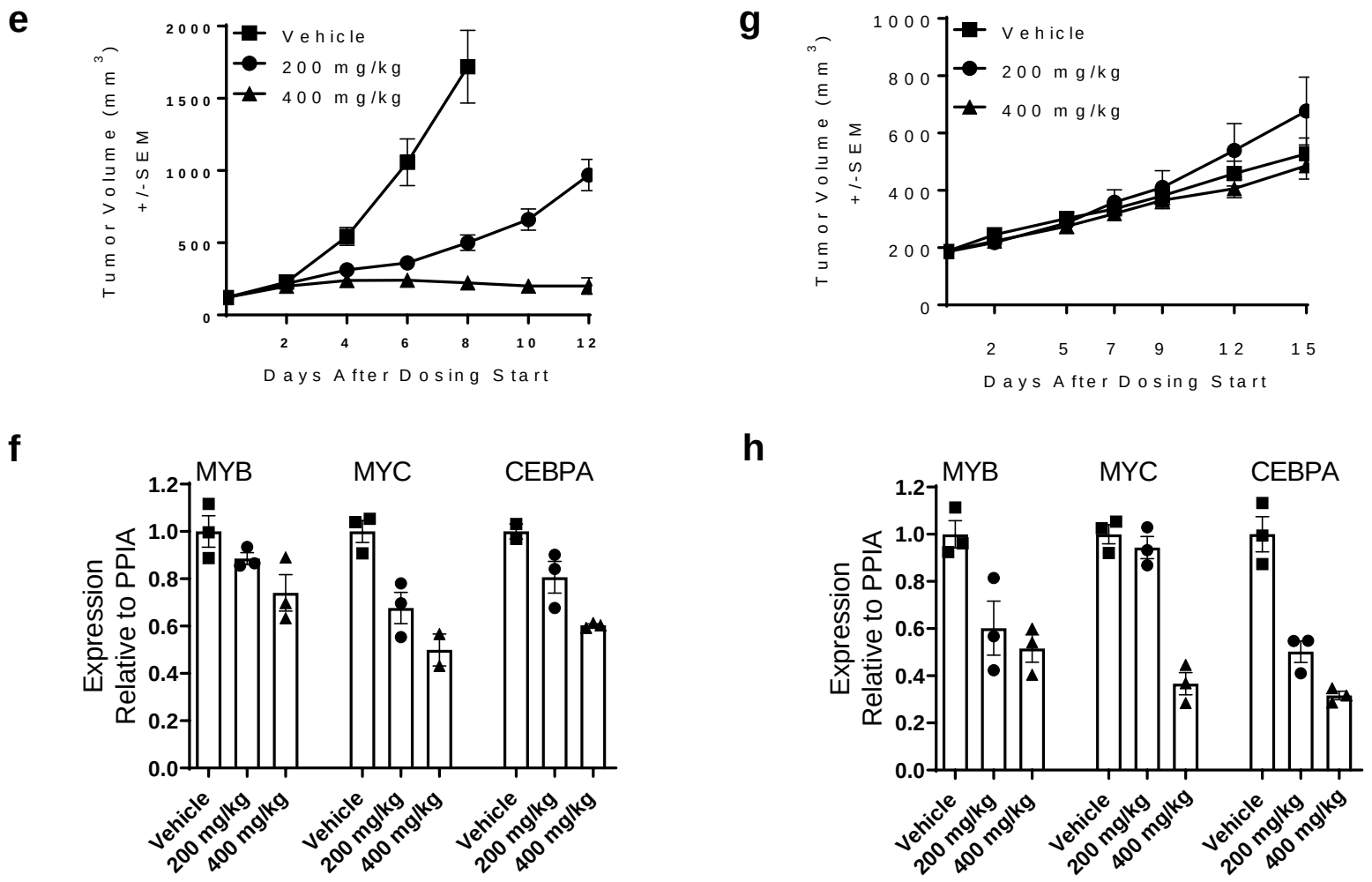

Supplementary Figure 4 continued: **e**, Tumor volume and **f**, biomarker expression by RT-qPCR in MOLM-13 mouse xenografts treated with compound **1**. **g**, Tumor volume and **h**, biomarker expression by RT-qPCR in mouse xenografts of A549 lung adenocarcinoma cells (compound insensitive, high CES1 expression) treated with compound **1**. For efficacy experiments, $2x10^6$ cells were implanted subcutaneously and allowed to grow until tumor volume reached 150-200 mm^3 (8 days for MOLM-13, 21 days for A549). **1** was dosed twice per day by subcutaneous injection. Relative quantification by comparative CT method was applied for all qPCR reactions, normalizing transcript quantities per target gene to those of endogenous control PPIA per sample and setting the vehicle-treated condition per target gene equal to 1. Center value presented as mean plus/minus standard error of mean, with eight animals per treatment group.

a

GO_term	FDR	Genes in network	Genes in genome	GO_term_type	GO_accession
termination of RNA polymerase II transcription	4.21E-47	25	45	biological_process	GO:0006369
mRNA 3'-end processing	2.06E-40	26	88	biological_process	GO:0031124
DNA-templated transcription, termination	6.25E-39	25	84	biological_process	GO:0006353
RNA 3'-end processing	6.47E-39	26	101	biological_process	GO:0031123
RNA splicing, via transesterification reactions with bulged adenosine as nucleophile	1.97E-28	25	208	biological_process	GO:0000377
mRNA splicing, via spliceosome	1.97E-28	25	208	biological_process	GO:0000398
RNA splicing, via transesterification reactions	3.47E-28	25	214	biological_process	GO:0000375
mRNA processing	3.47E-28	27	288	biological_process	GO:0006397
RNA splicing	1.61E-25	25	274	biological_process	GO:0008380
nucleic acid transport	1.08E-18	15	85	biological_process	GO:0050657
RNA transport	1.08E-18	15	85	biological_process	GO:0050658
RNA localization	1.08E-18	15	84	biological_process	GO:0006403
establishment of RNA localization	1.08E-18	15	85	biological_process	GO:0051236
mRNA export from nucleus	2.46E-18	14	68	biological_process	GO:0006406
mRNA transport	2.87E-18	14	69	biological_process	GO:0051028
RNA export from nucleus	1.18E-17	14	76	biological_process	GO:0006405
nucleobase-containing compound transport	2.81E-17	15	106	biological_process	GO:0015931
nuclear export	3.77E-15	14	113	biological_process	GO:0051168
mRNA cleavage factor complex	4.78E-12	7	12	cellular_component	GO:0005849
RNA polyadenylation	1.33E-11	8	24	biological_process	GO:0043631

b

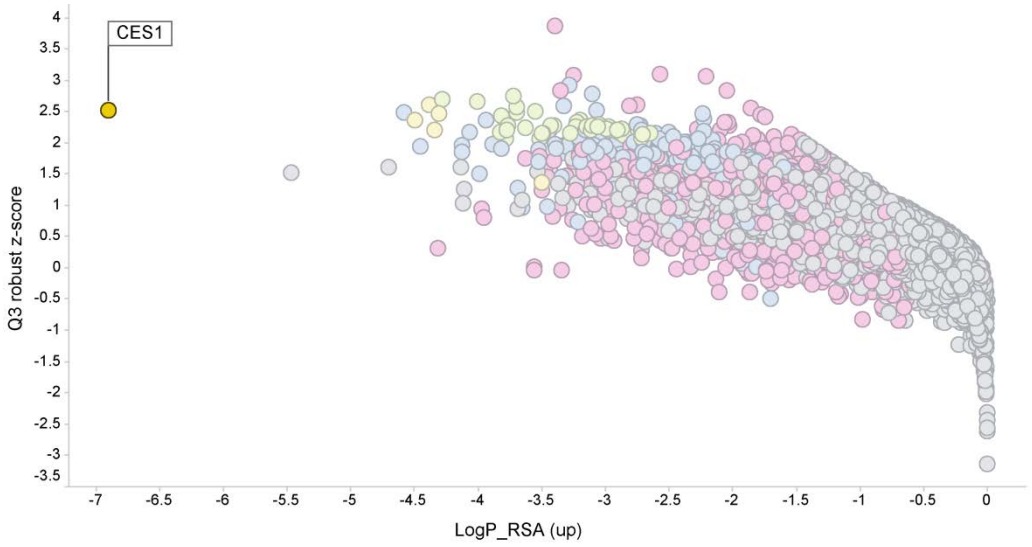

Supplementary Figure 5: Genome-wide siRNA plus compound synergy screen. The siRNA library was tested as one replicate with each gene represented by n=8 siRNAs on average per condition. **a**, 20 most highly enriched GO terms from GeneMANIA analysis of top 50 gene candidates (compound **1** minus DMSO analysis). **b**, Full genome siRNA plus compound **1** synergy screen in A-673 cells, with cell viability read-out via CellTiter Glo assay, as shown in Figure 2a, but here plotting of redundant siRNA activity (RSA statistical model, one-sided, up) versus Q3 Z-score to identify siRNA-targeted genes whose knock-down desensitized cells to compound **1** treatment. Top screening hit CES1 labeled.

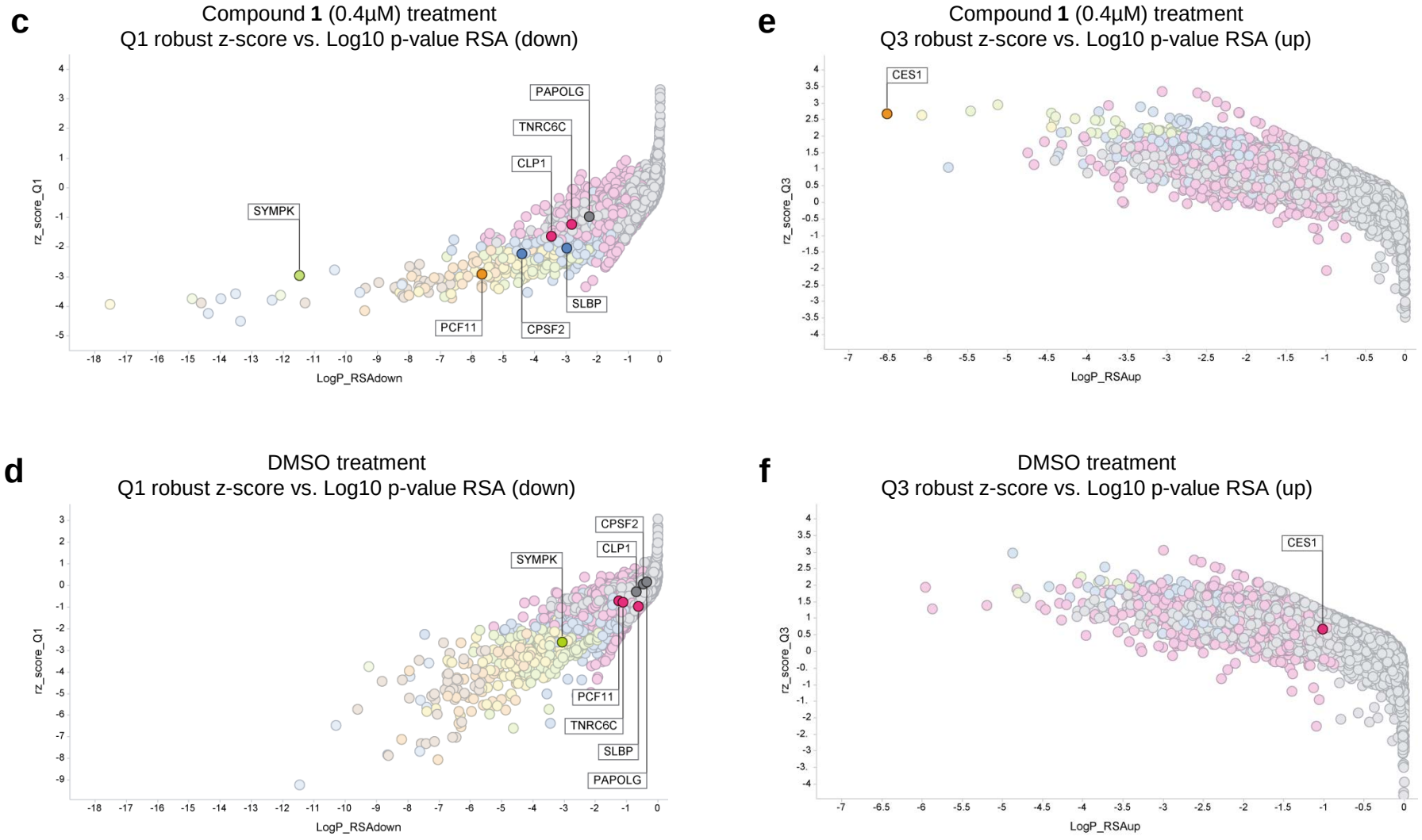

Supplementary Figure 5 continued: c-f, Gene-level activity in individual screening conditions as indicated. Known regulators of mRNA processing (RSA statistical model, one-sided, down versus Q1) as well as CES1 (RSA statistical model, one-sided, up versus Q3) are highlighted and named.

a

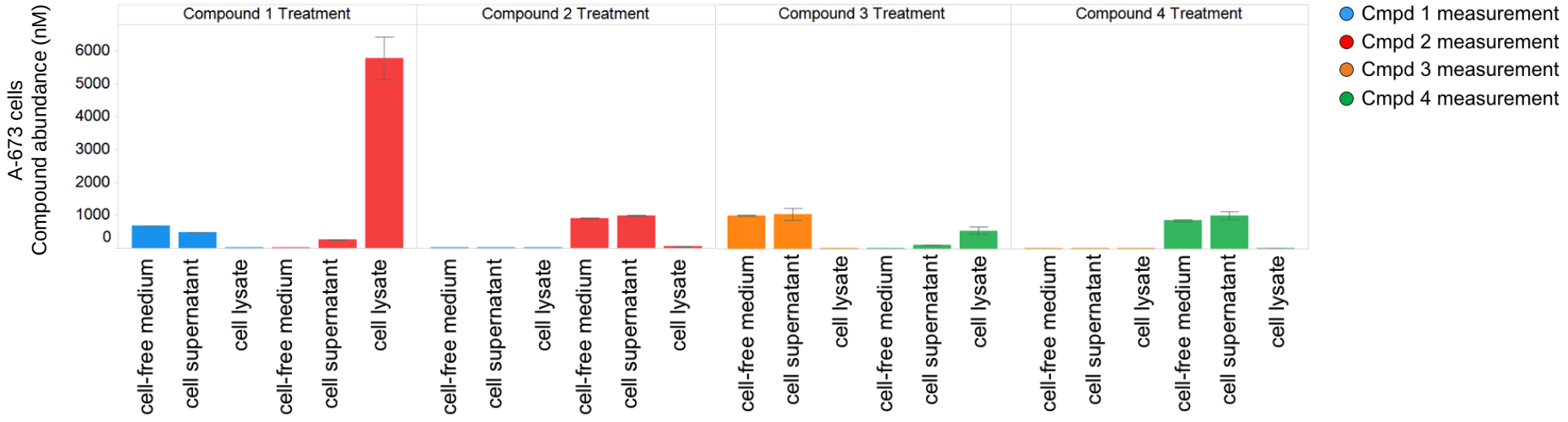

b

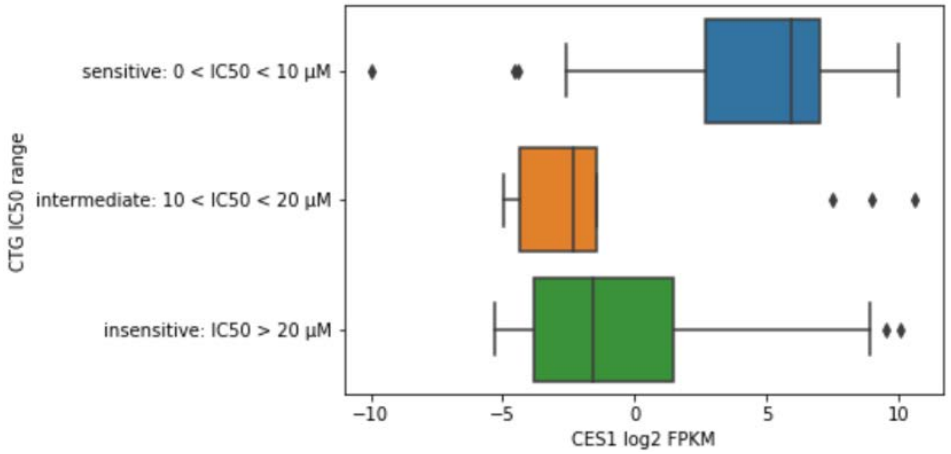

cell_viability_ctg_assay_ic50_range	count	mean	std	min	25%	50%	75%	max
insensitive: IC50 > 20 ¬µM	33	-0.256780663	4.705832014	-5.288398479	-3.841009155	-1.602478555	1.489078884	10.05994969
intermediate: 10 < IC50 < 20 ¬µM	13	-0.383578782	5.548321975	-4.971039387	-4.33566764	-2.342195007	-1.422455742	10.63364717
sensitive: 0 < IC50 < 10 ¬µM	29	4.362697636	4.829708908	-9.965784285	2.688829832	5.965276354	6.988612272	10.01360107

Supplementary Figure 6:

c

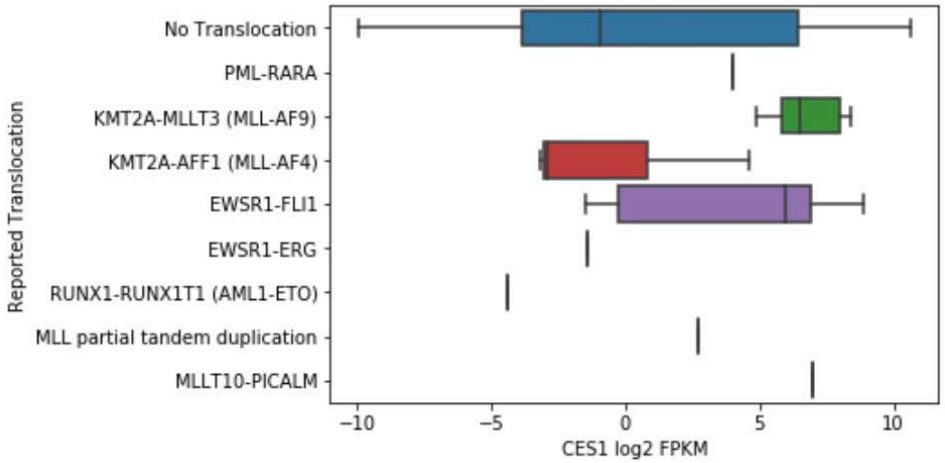

transloc	count	mean	std	min	25%	50%	75%	max
EWSR1-ERG	1	-1.422455742		-1.422455742	-1.422455742	-1.422455742	-1.422455742	-1.422455742
EWSR1-FLI1	5	3.99409302	4.578493264	-1.485170226	-0.248255271	5.965276354	6.891957358	8.846656884
KMT2A-AFF1 (MLL-AF4)	3	-0.511452519	4.410127831	-3.193600633	-3.056408698	-2.919216763	0.829621539	4.57845984
KMT2A-MLLT3 (MLL-AF9)	5	6.722386443	1.492343251	4.85184068	5.83895357	6.482208176	8.008769571	8.430160218
MLL partial tandem duplication	1	2.688829832		2.688829832	2.688829832	2.688829832	2.688829832	2.688829832
MLLT10-PICALM	1	6.988612272		6.988612272	6.988612272	6.988612272	6.988612272	6.988612272
No Translocation	57	0.933014101	5.519291564	-9.965784285	-3.841009155	-0.915516826	6.422854329	10.63364717
PML-RARA	1	3.991000923		3.991000923	3.991000923	3.991000923	3.991000923	3.991000923
RUNX1-RUNX1T1 (AML1-ETO)	1	-4.417885379		-4.417885379	-4.417885379	-4.417885379	-4.417885379	-4.417885379

Supplementary Figure 6: **a**, A-673 compound sensitive cells treated with compound **1**, **2**, **3**, or **4** for 4h. The presence or appearance of each compound were measured by mass spectrometry in media without cells (cell-free media), media from wells containing cells (cell supernatant), or from lysates of washed cell pellets (cell lysate). Center value represents mean and error bars represent standard deviation (n=3). **b**,**c**, Comparison of CES1 mRNA expression to (**b**) sensitivity to compound **1** across 92 cell line panel or to (**c**) reported translocation status among AML and Ewing's sarcoma cell lines tested. Boxplots in (**b**,**c**) represent Median bounded by Q1 and A3, with bars extended to cover the standard deviation.

a

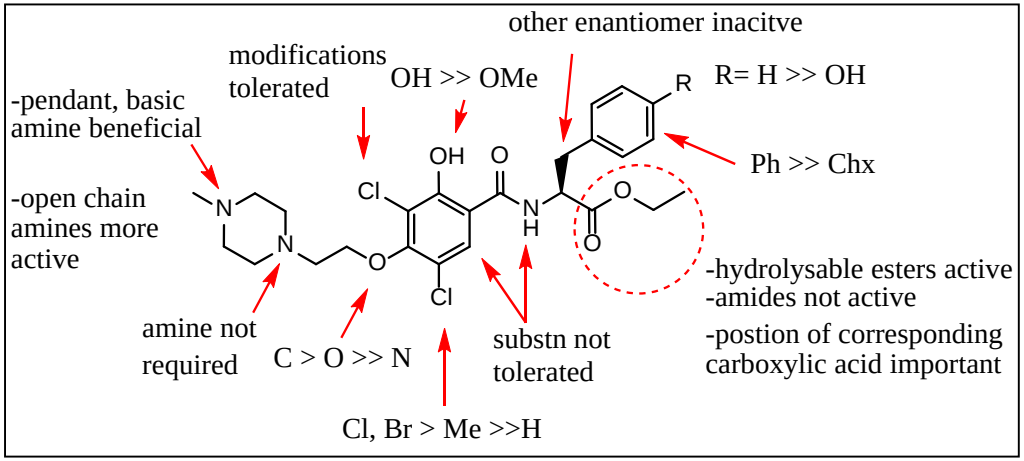

b

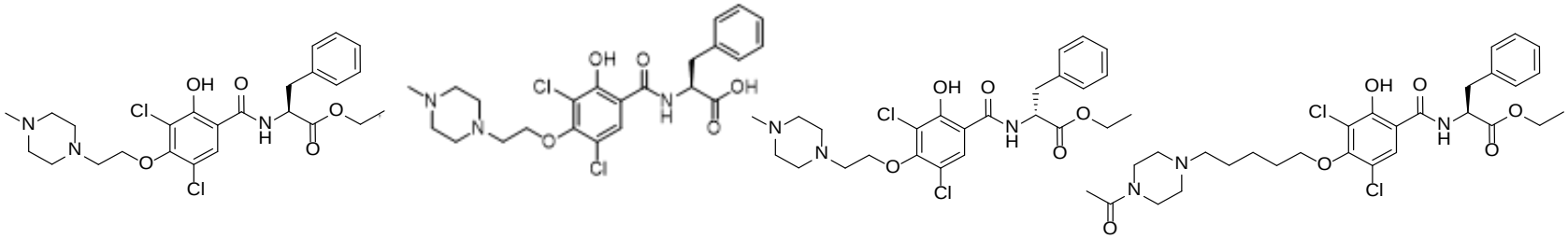

	1		**2**		**3**		**5**	
AML cell lines sensitive to compound **1**	MOLM-13:	0.27 µM	MOLM-13:	0.43 µM*	MOLM-13:	>30 µM	MOLM-13:	0.18 µM
	NOMO-1:	0.48 µM	NOMO-1:	>30 µM	NOMO-1:	>30 µM	NOMO-1:	0.32 µM
AML cell lines not sensitive to compound **1**	CMK:	>30 µM	CMK:	>30 µM	CMK:	>30 µM	CMK:	>30 µM
	HEL92.1.7	>30 µM	HEL92.1.7	>30 µM	HEL92.1.7	>30 µM	HEL92.1.7	>30 µM
Ewing's sarcoma sensitive to compound **1**	A-673:	0.55 µM	A-673:	>30 µM	A-673:	>30 µM	A-673:	2.3 µM
	SK-ES-1:	0.60 µM	SK-ES-1:	>30 µM	SK-ES-1:	>30 µM	SK-ES-1:	2.5 µM

* partial activity

Supplementary Figure 7: **a**, Structure-activity relationships for compound **1**. **b**, IC_{50} values for compounds as indicated, derived from cell viability (CellTiter Glo) experiments across six cell lines used for compound optimization and SAR.

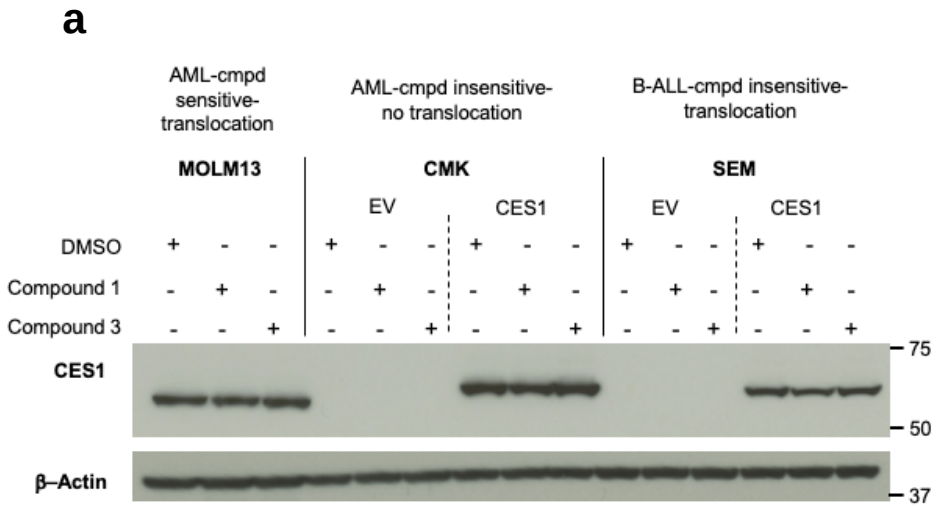

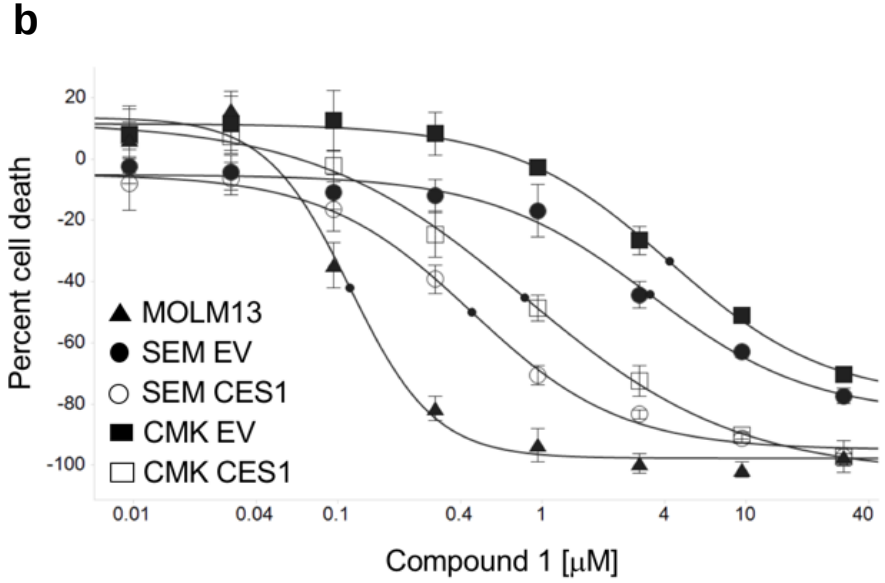

Supplementary Figure 8: **a**, Western blot assay to assess CES1 protein expression following stable viral transduction of human CES1 cDNA into CMK or SEM cell lines, with empty vector (EV) transduction as control. Treatment with 10μM compound **1** or **3** or DMSO as indicated. Non-transfected MOLM13 cell line shown for comparison (n=2). An uncropped scan of this blot is provided in Supplementary Figure 21a. **b**, Cell viability assessment of CES1 versus EV transduced CMK and SEM cell lines as indicated in response to compound 1 treatment in 8-point dose-response, with non-transfected MOLM13 cell line assayed in parallel (n=6, center point represents mean, error bars represent standard deviation, small black dots on fitted curves represent IC_{50} values).

Input material: 5 mg Nomo-1 (9:1 S0.8+P0.8; no benzonase treatment)
Affinity matrix: Compound **6**
Competition compound: 0 (-) or 100 µM (+) compound **2**

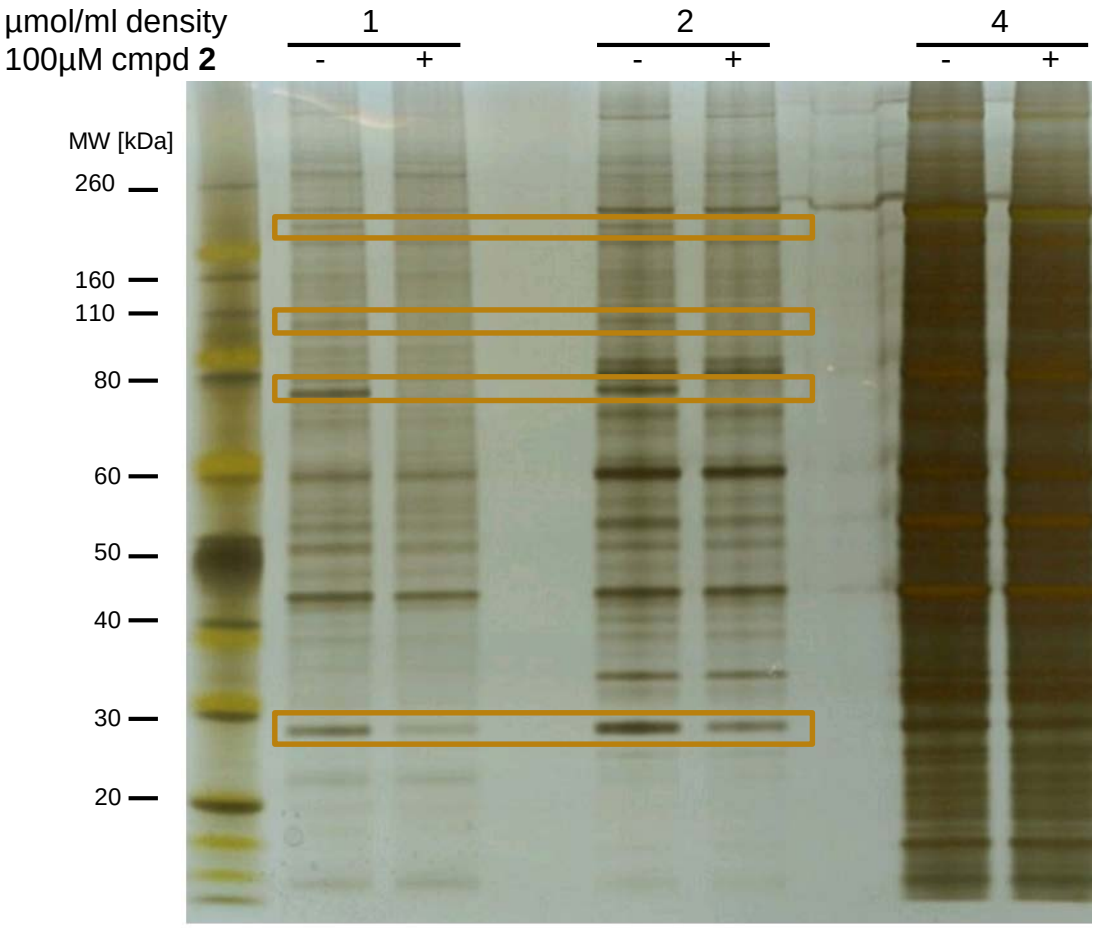

Supplementary Figure 9: Bioactive linker analog coupled to sepharose resin to give affinity matrix **6** incubated with NOMO-1 cell lysate. 1 and 2 µmol/ml coupling densities allow for protein pull-down and competition by free compound **2** as observed by silver stain SDS-PAGE (n=1). Boxed bands indicate proteins specifically competed with free compound.

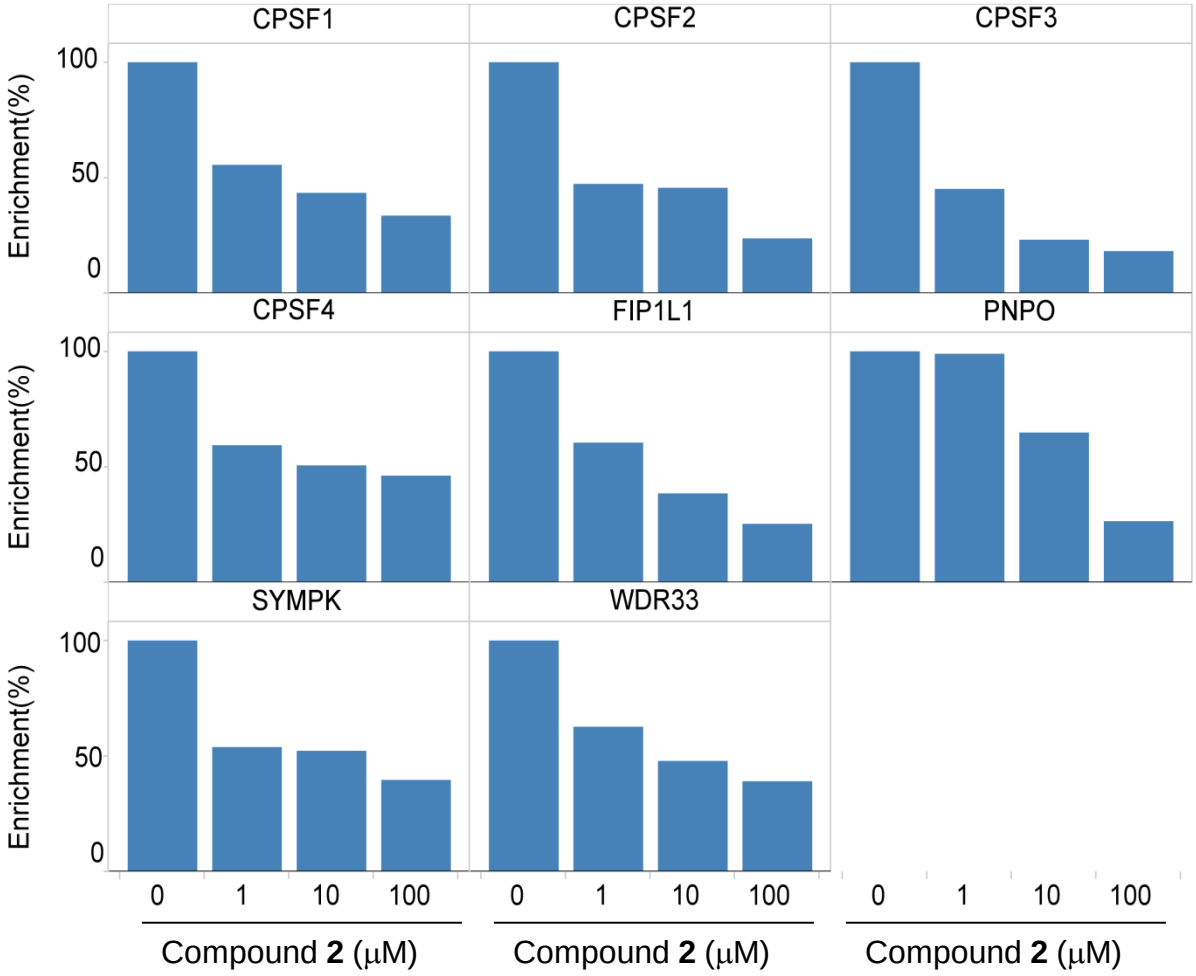

Supplementary Figure 10: Top hits from affinity pulldown experiment in NOMO-1 cells are concentration-dependent binders as determined by compound **2** competition with the affinity matrix **6**.

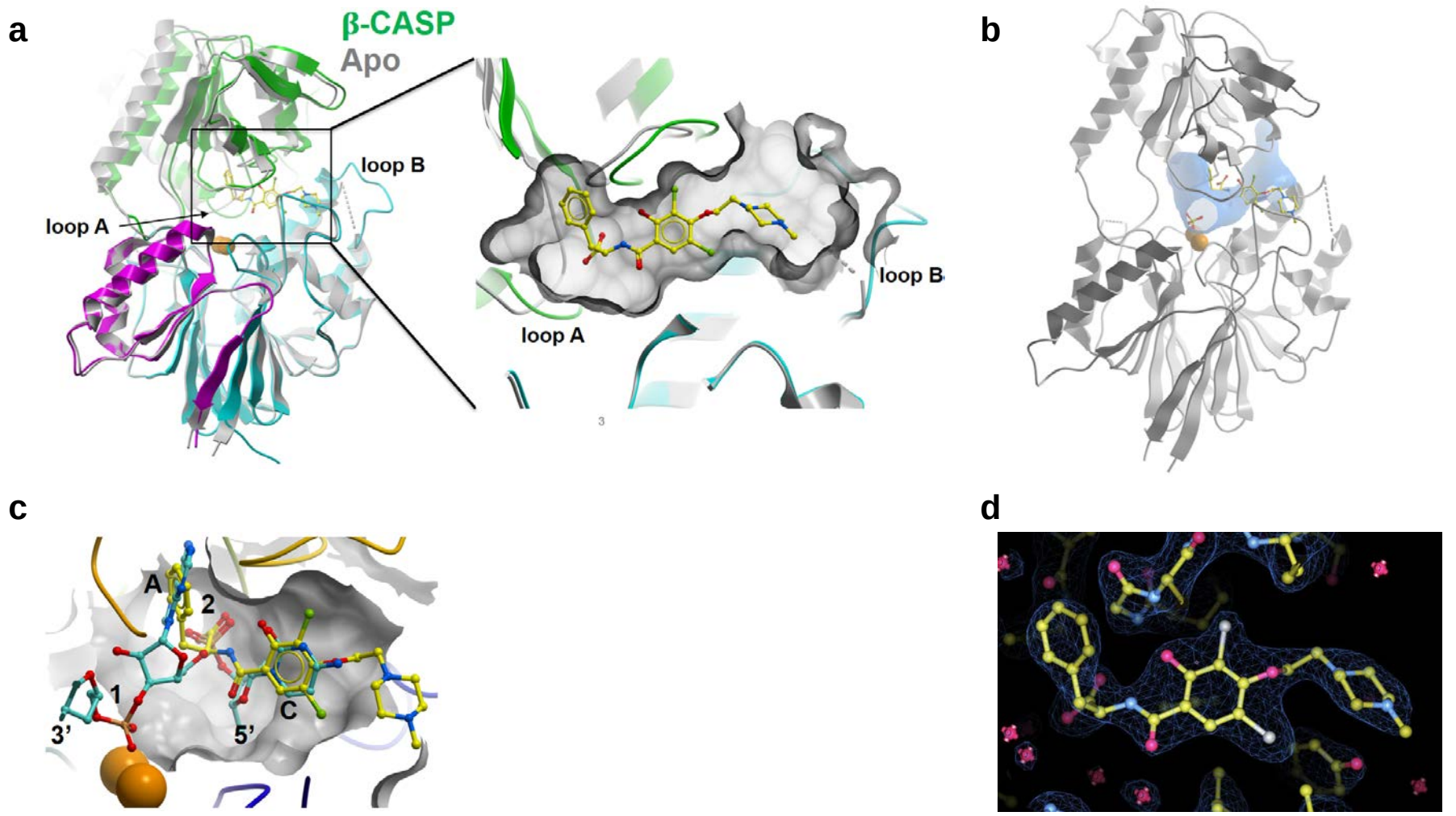

Supplementary Figure 11: CPSF3 co-crystal structure with compound **2**. **a**, Domain rotation and conformational changes of CPSF3 upon binding of **2** (yellow). Apo CPSF3 (pdb code 2I7T) is shown in ribbon representation in grey and CPSF3 bound to **2** is colored according to Figure 3a. The large metallo-β-lactamase domains of both structures were aligned (grey and blue) and the β-CASP domains were allowed to move freely. Overall, the β-CASP domain (green) shows a 7.3 degree rotation upon binding of **2**. Loop regions lining the domain interfacial cavity show structural rearrangements upon ligand binding, the most significant changes were observed for loop A and B. **b**, Active site cavity (blue volume) in apo CPSF3. Position of compound **2** shown for comparison. A sulfate coordinates the two zinc ions. **c**, Model of a CA RNA fragment (cyan) bound to the active site of CPSF3. Phosphodiester 1 was overlaid with the zinc-coordinating phosphate observed in crystal structures of **2**-bound CPSF3. Phosphodiester 2 was placed at the carboxylate position of **2**. Adenine and cytosine were overlaid with the phenyl and hydroxy-dibromo-phenyl groups of **2**, respectively. **d**, $2F_o$-F_c electron density for compound **2** contoured at 1.4σ.

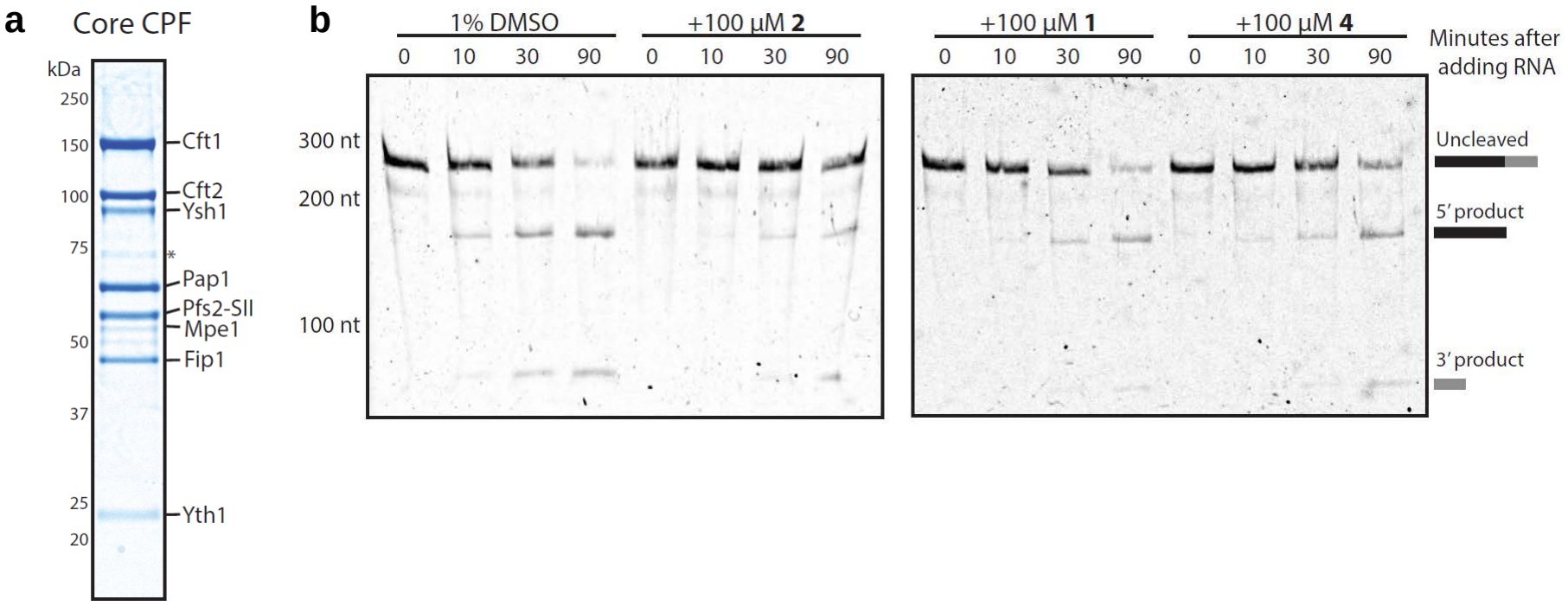

Supplementary Figure 12: Compound **2** inhibits the endonuclease activity of yeast core CPF. **a**, Recombinant 8-subunit core CPF complex was purified from insect cells. 5 µl were resolved by SDS-PAGE and stained with Coomassie. **b**, 6% TBE-Urea PAGE gels of 259 nt *Cyc1* RNA substrate cleavage reactions treated with 100 µM compound **2**, **1**, **4** or 1% DMSO. Gels were stained with SYBR Green II. Shown are one set of representative gels from three independent experiments.

a

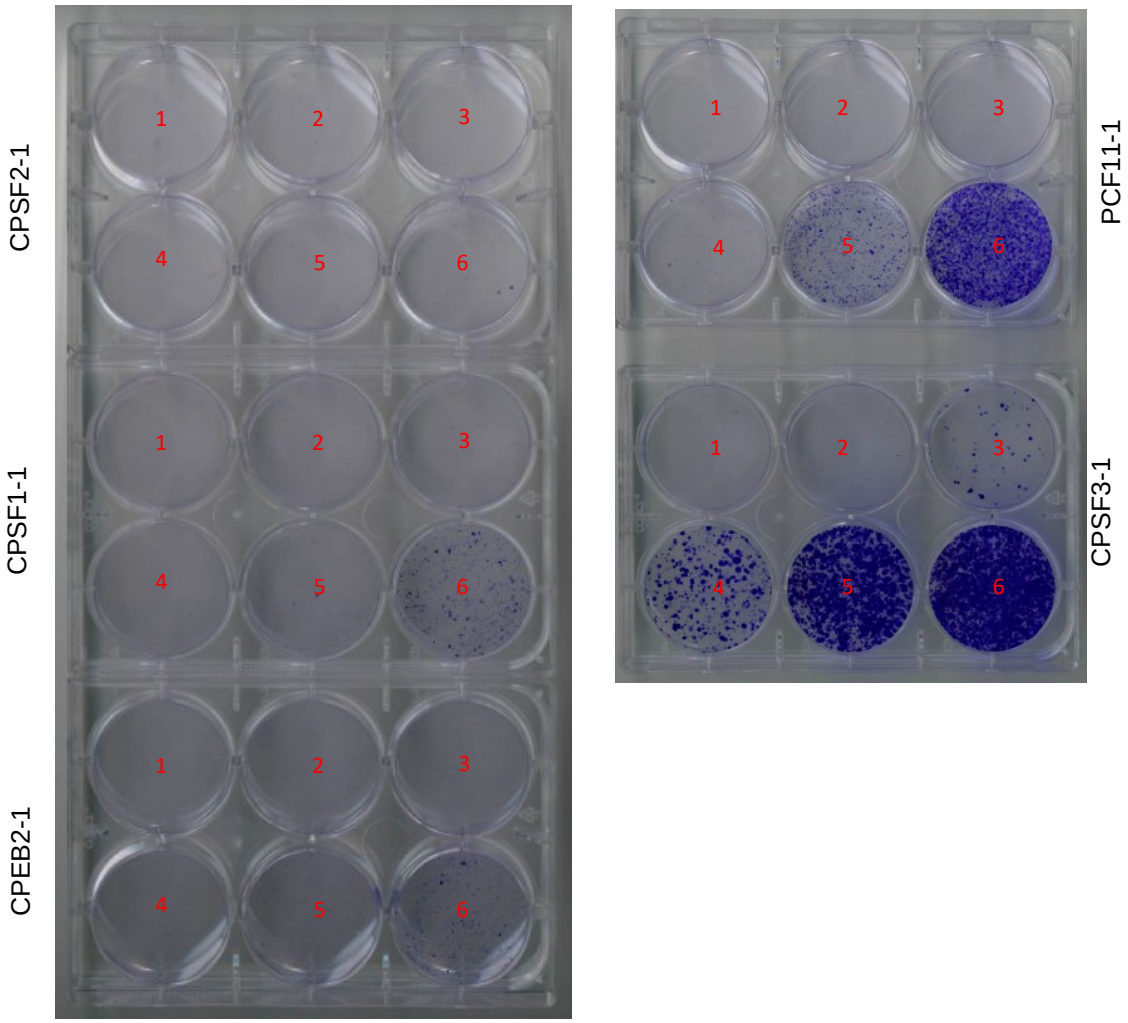

- ❑ Day 1: Seeded 8,000/well stably infected A-673 cells.
- ❑ Day 3: Added compound **1** in dose-response as indicated.
- ❑ Day 10: Fixed and stained cells.

6w-plate well number	Compound 1 (μM)
1	50
2	25
3	12.5
4	6.25
5	3.125
6	1.5625

Supplementary Figure 13: **a**, Functional variomics of top 14 candidate compound targets in colony formation assays *in vitro* using A-673 cells treated with compound **1** as indicated (repeated independently two times).

a

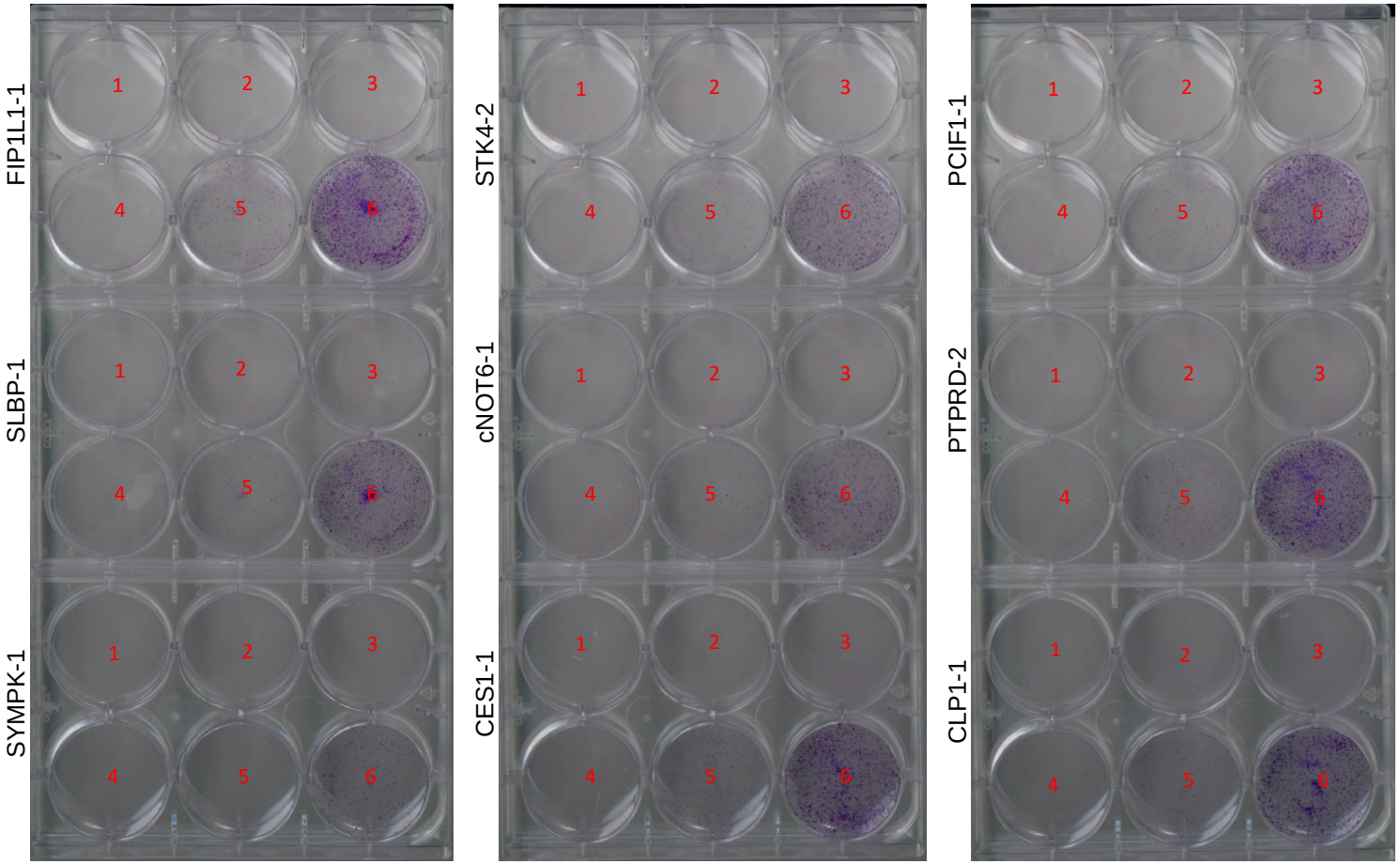

Supplementary Figure 13 continued: **a**, Functional variomics of top 14 candidate compound targets in colony formation assays *in vitro* using A-673 cells treated with compound **1** as indicated.

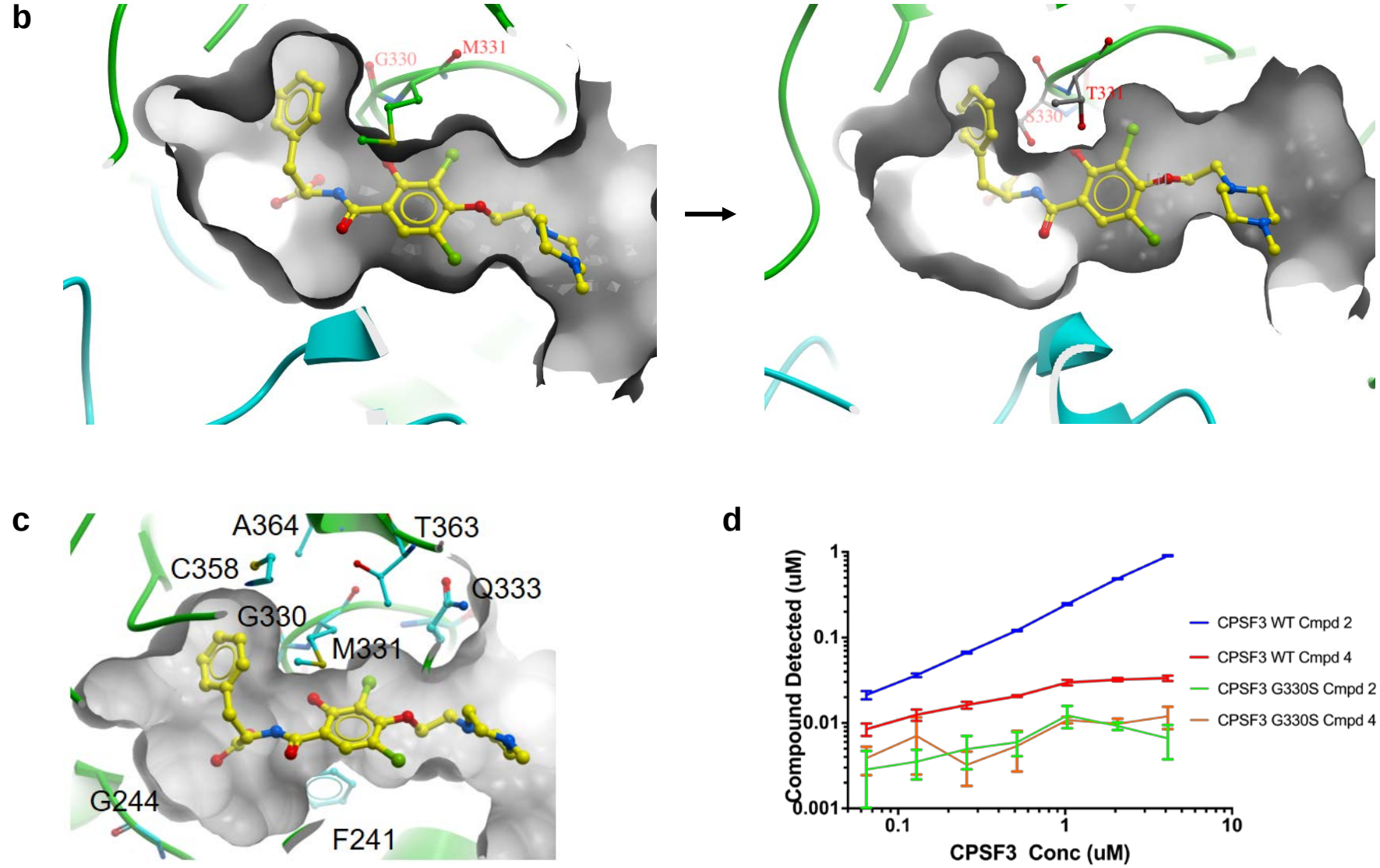

Supplementary Figure 13 continued: **b**, The two most prevalent missense mutations Gly330Ser, Met331Thr/Val modeled onto X-ray structure are predicted to constrict the compound **2** binding pocket while retaining catalytic activity. **c**, Positions of most frequently mutated residues (count > 4) cluster in the small β-CASP domain of CPSF3 (top), and are in close proximity to the binding site of **2**. **d**, Affinity binding measurement of compound **2** or **4** to human CPSF3 wild-type (WT) or G330S mutant protein as determined by SEC-TID. Error bars represent standard deviation of the mean (n=3).

e

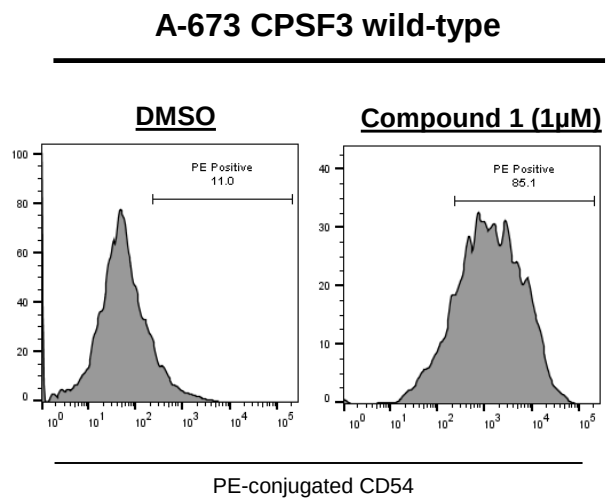

f

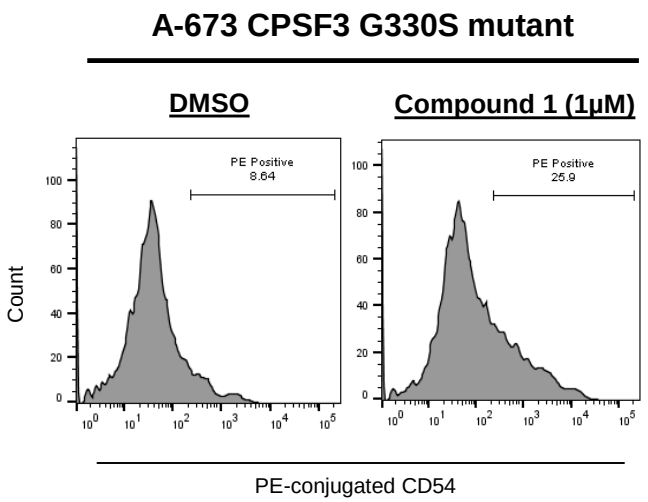

Supplementary Figure 13 continued: **e**,**f**, FACS analysis of cell surface CD54 expression in response to compound **1** treatment comparing (**e**) A-673 cells with CPSF3 wild-type to (**f**) variomics-derived A-673 cells expressing the CPSF3 G330S mutant (repeated independently two times).

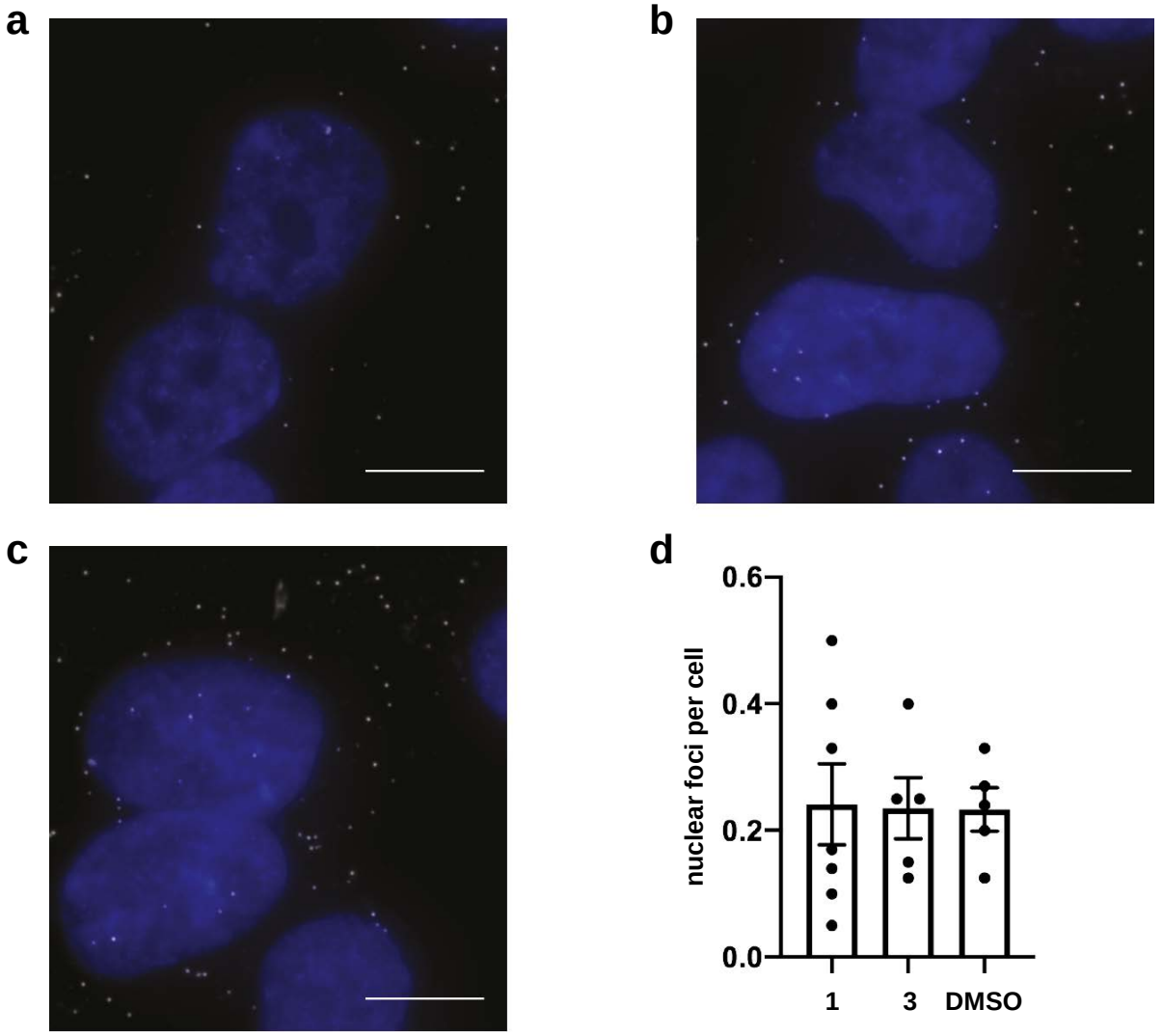

Supplementary Figure 14: **a**,**b**,**c**, Images of A-673 cells that were treated with compound **1** (**a**), compound **3** (**b**) or DMSO (**c**) for four hours prior to fixation and probed for RUNX-3 mRNAs (white) using FISH probes targeted to the coding sequence of the transcript. Nuclei (blue) were stained with DAPI. Images are representative from three independent experiments performed in duplicate. Scale bar = 10μm. **d**, Similar numbers of nuclear foci of RUNX-3 transcripts were detected in cells treated with DMSO (52 cells), compound **1** (41 cells) or compound **3** (44 cells) (p-value 0.98, one-way ANOVA). Data are presented as mean plus/minus standard error of mean for nuclear foci counted in each experiment.

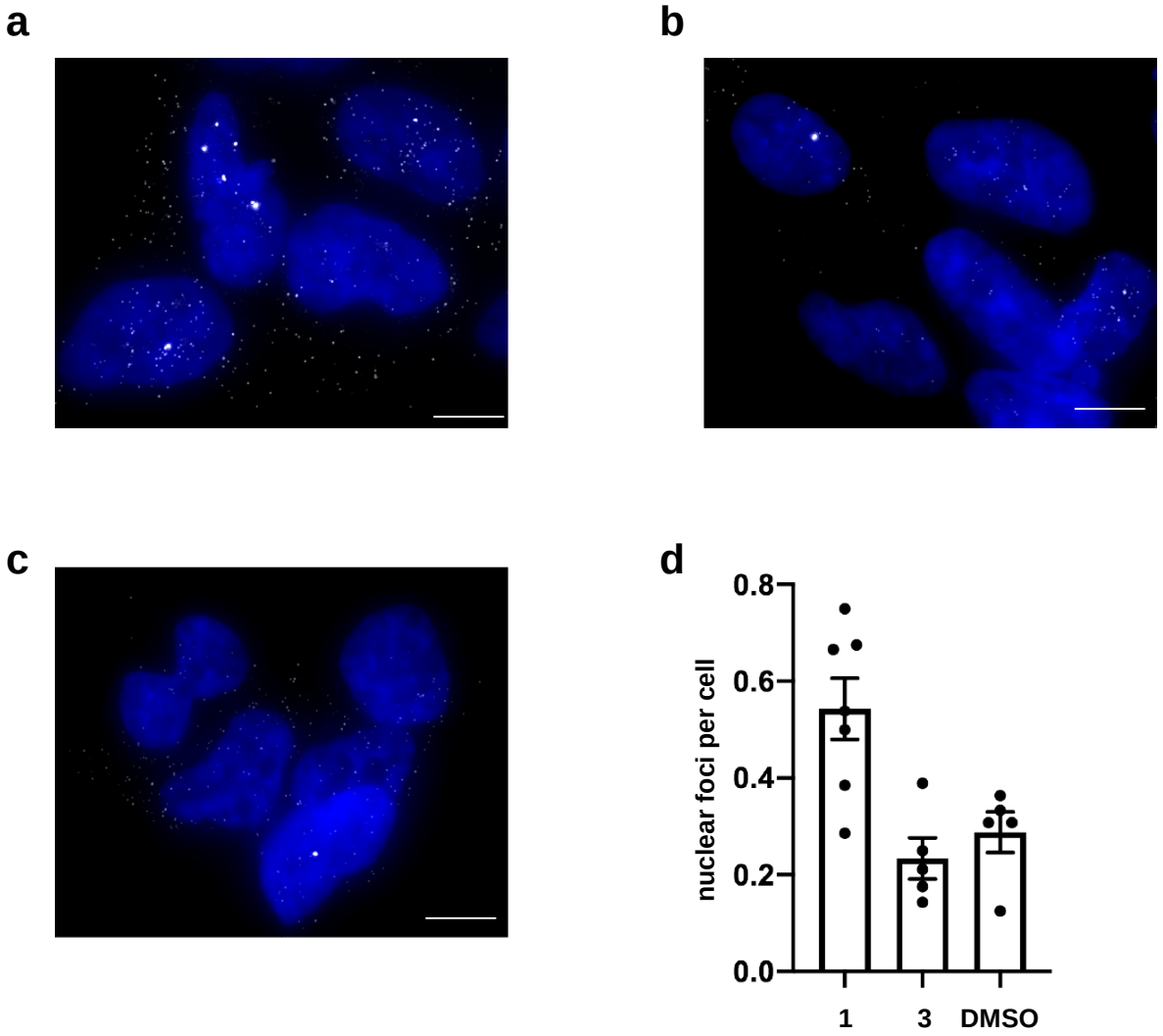

Supplementry Figure 15: **a**,**b**,**c**, Images of A-673 CPSF3 G330S cells that were treated with compound 1 (**a**), compound 3 (**b**) or DMSO (**c**) for 4 h prior to fixation and probed for NKX2-2 mRNAs (white) using FISH probes targeted to the coding sequence of the transcript. Nuclei (blue) were stained with DAPI. Images are representative from two independent experiments performed in duplicate. Scale bar = 10μm. **d**, Quantification of the number of NKX2-2 nuclear foci in cells treated with compound 1 (85 cells), compound 3 (80 cells) and DMSO (54 cells). Data are presented as mean plus/minus standard error of mean for nuclear foci counted in each experiment.

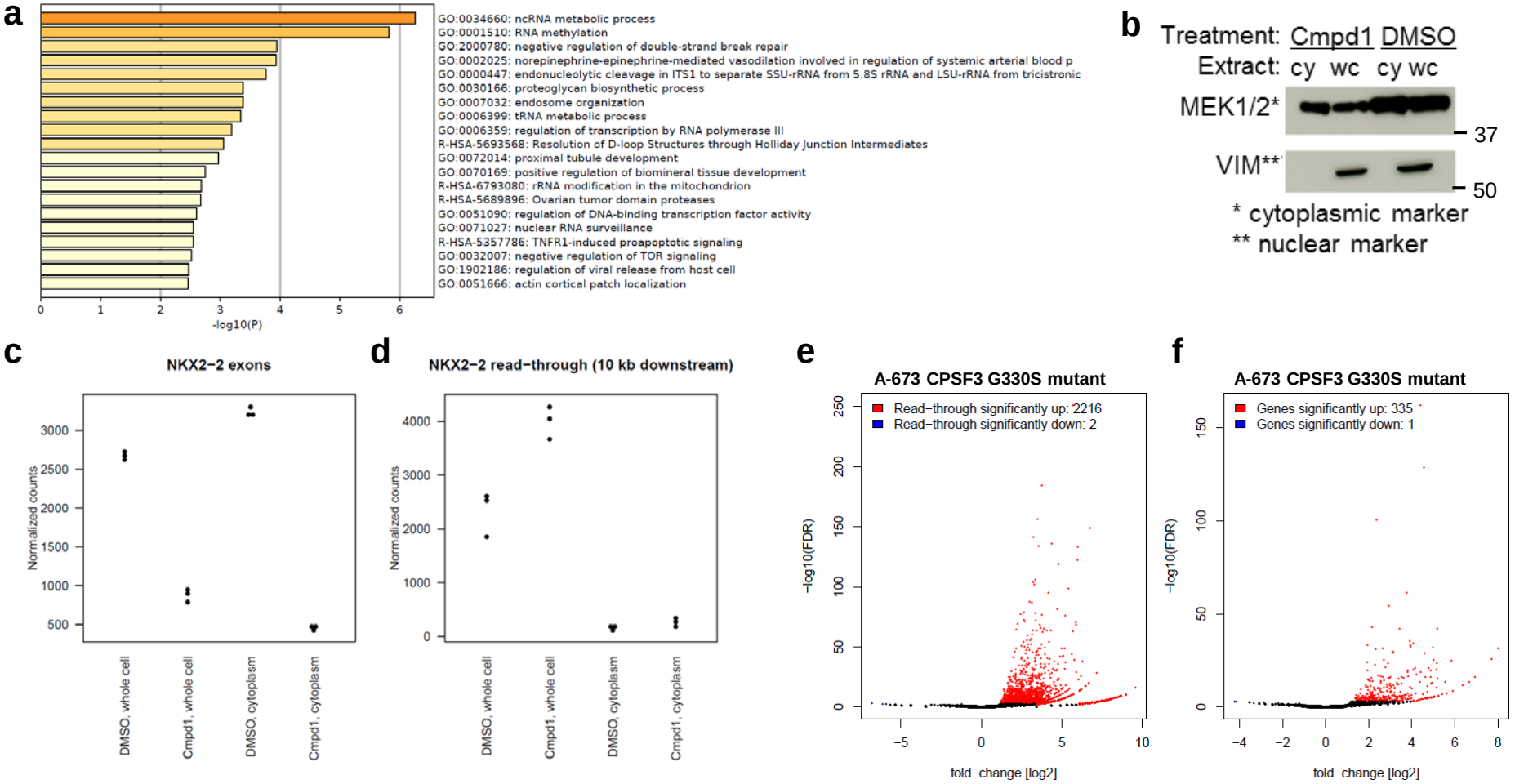

Supplementary Figure 16: **a**, Pathway and process enrichment using Metascape among genes significantly downregulated with 10μM compound **1** in A-673 cells based on RNA-seq expression profiling from whole cell extract (as shown in Figure 4g). Geneset enrichments were calculated using the hypergeometric test and Benjamini-Hochberg multiple comparison adjustment via Metascape. **b**, Protein expression analysis by Western blot against MEK1/2 as a cytoplasmic marker and Vimentin as a nuclear marker in cytoplasmic (cy) extracts or whole cell (wc) extracts to assess purity of subcellular fractionation (n=1). An uncropped scan of this blot if provided in Supplemental Figure 21b. **c**,**d**, NKX2-2 exonic (**c**) versus read-through (**d**) expression levels quantified by RNA-seq in A-673 cells treated with **1** or DMSO for 4 h prior to RNA purification from either whole cell or cytoplasmic extracts, with three biological replicates per condition. **e**,**f**, RNA-seq based quantification of (**e**) read-through expression genome-wide and of (**f**) changes in global gene expression in A-673 Variomics-derived CPSF3 G330S mutant cells, upon 4 h treatment with 10 μM **1** versus DMSO analyzing RNA purified from whole cell extracts of three biological replicates. Normalized read counts were analyzed using a negative binomial generalized log-linear model with two-sided comparisons and false discovery rate controlled using Benjamini-Hochberg multiple comparisons adjustment via edgeR. Significance cut-offs defined as absolute value fold-change [log2] > 1 and adjusted p-val/FDR < 0.05.

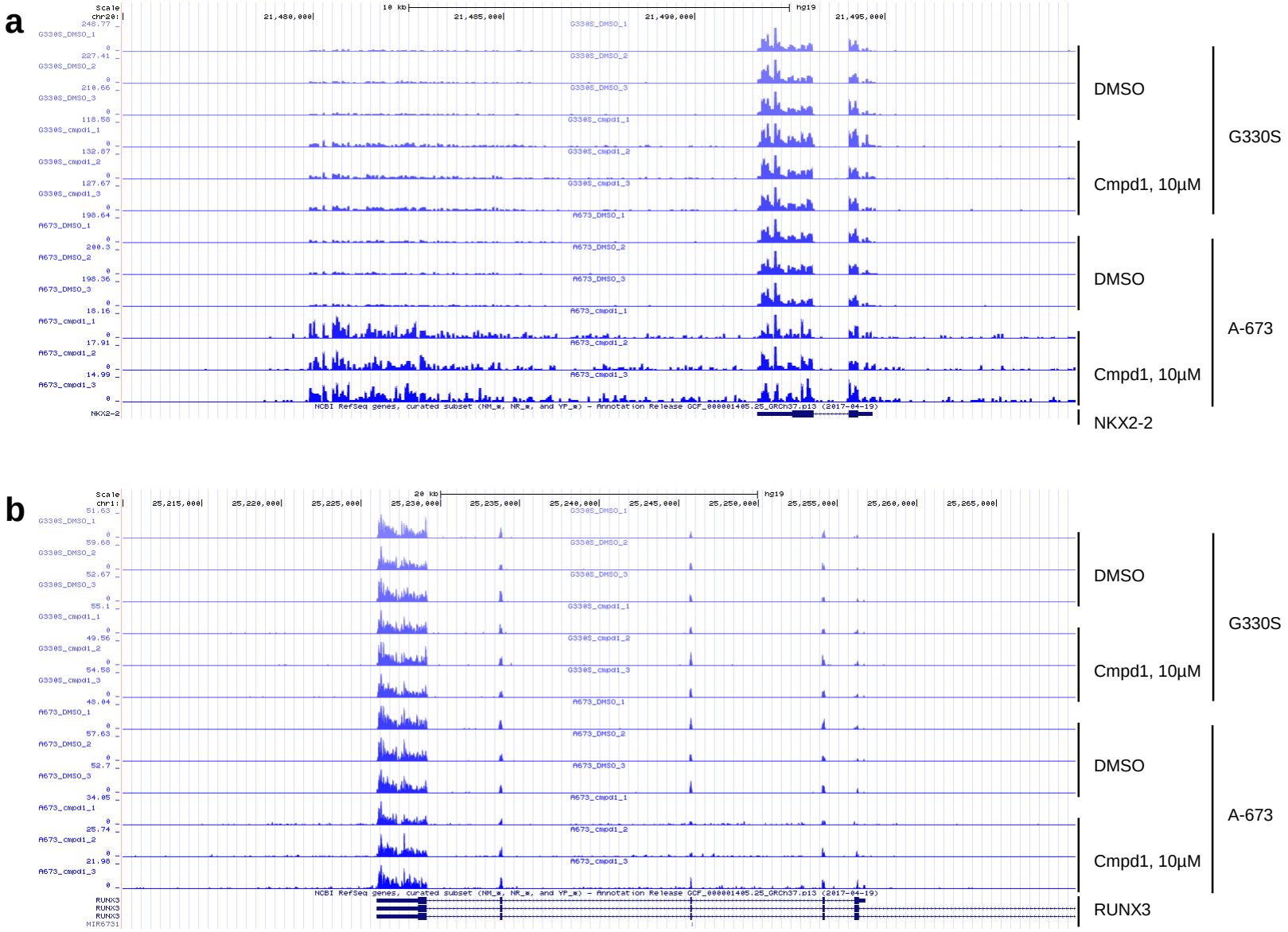

Supplementary Figure 17: RNA-seq traces comparing 4h compound **1** treatment (10µM) to DMSO control in either A-673 or CPSF3 G330S mutant expressing cells. Dynamic scaling of y-axis to visualize degree of transcript read-through at 3′-UTR and beyond in relation to read coverage at exons. **a**, NKX2-2 locus, hg19 chr20:chr20:21,475,000-21,500,000 and **b**, RUNX3 locus, hg19 chr1:25,210,000-25,270,000. Three separate tracks are shown per condition reflecting replicate samples.

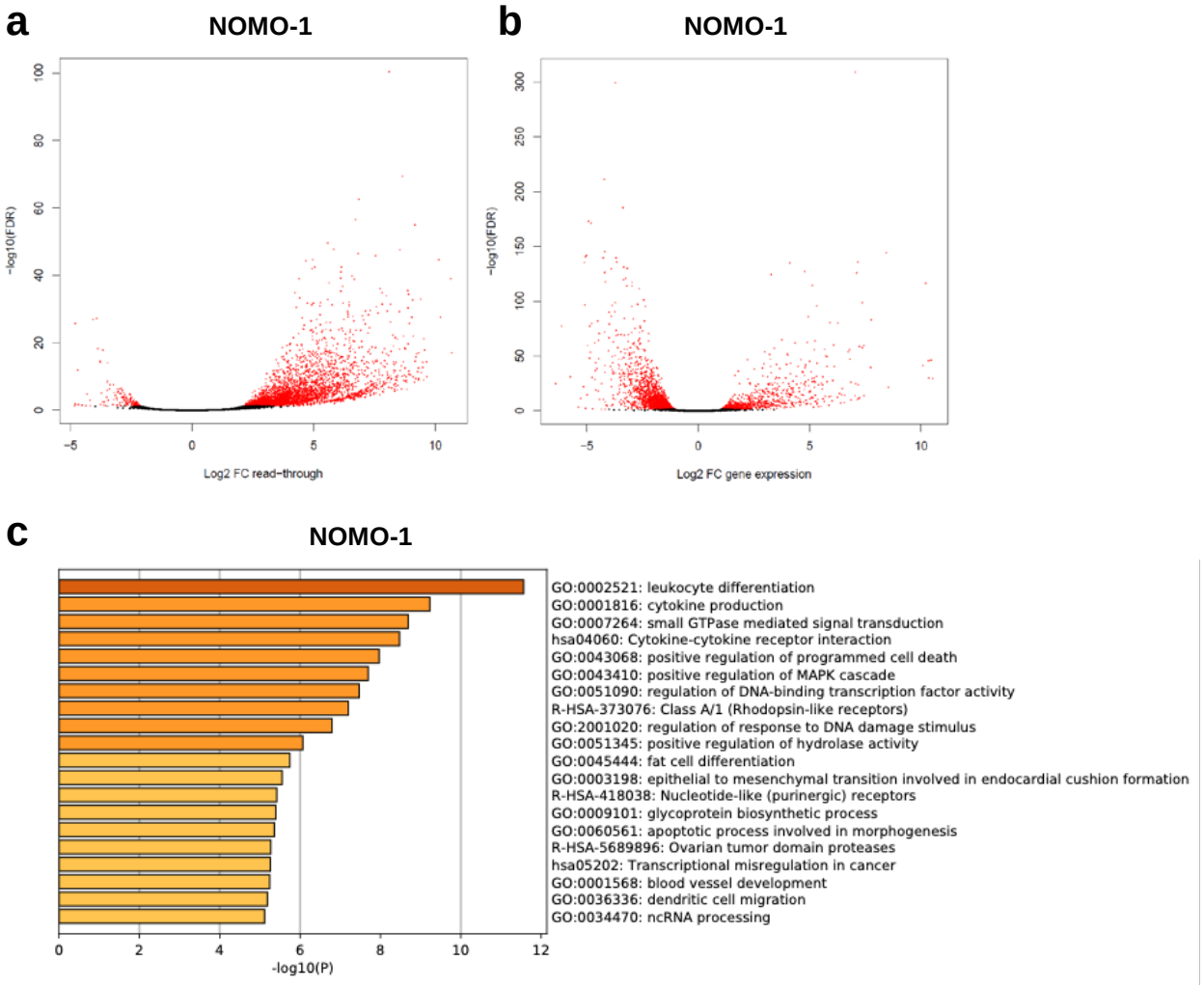

Supplementary Figure 18: **a**,**b**, RNA-seq based quantification in NOMO-1 cells of read-through expression genome-wide (**a**) and of changes in global gene expression in (**b**), both upon 4 h treatment with 10µM of **1** versus DMSO. Normalized read counts were analyzed using a negative binomial generalized log-linear model with two-sided comparisons and false discovery rate controlled using Benjamini-Hochberg multiple comparisons adjustment via edgeR. Significance cut-offs marked in red defined as absolute value fold-change [log2] > 1 and adjusted p-val/FDR < 0.05. **c**, Pathway and process enrichment using Metascape among genes significantly downregulated with 10µM compound 1 in NOMO-1 cells. Geneset enrichments were calculated using the hypergeometric test and Benjamini-Hochberg multiple comparison adjustment via Metascape. All analyses utilized RNA purified from whole cell extracts of three biological replicates.

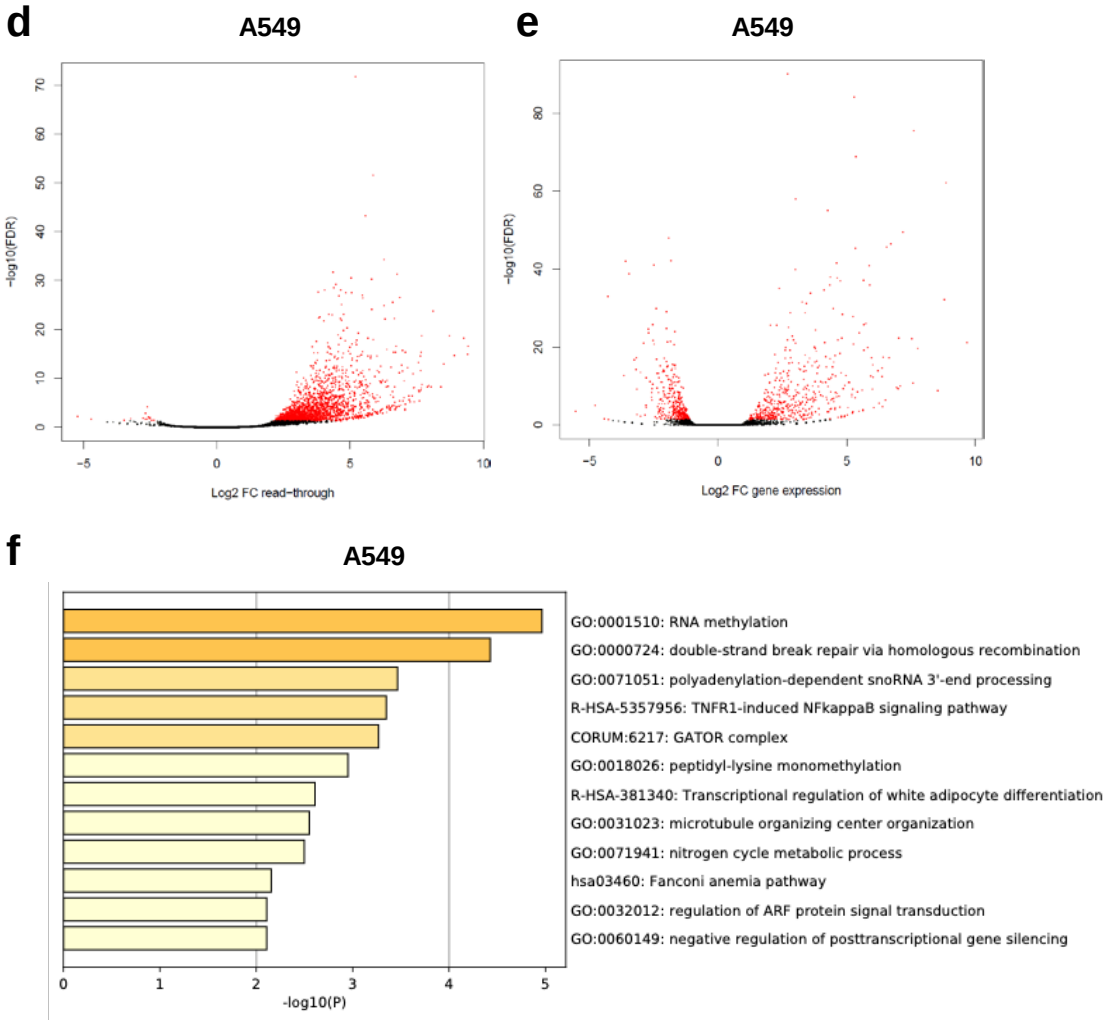

Supplementary Figure 18 continued: **d**,**e**, RNA-seq based quantification in A549 cells of read-through expression genome-wide (**d**) and of changes in global gene expression in (**e**), both upon 4 h treatment with 10µM of **1** versus DMSO. Normalized read counts were analyzed using a negative binomial generalized log-linear model with two-sided comparisons and false discovery rate controlled using Benjamini-Hochberg multiple comparisons adjustment via edgeR. Significance cut-offs marked in red defined as absolute value fold-change [log2] > 1 and adjusted p-val/FDR < 0.05. **f**, Pathway and process enrichment using Metascape among genes significantly downregulated with 10µM compound 1 in A549 cells. Geneset enrichments were calculated using the hypergeometric test and Benjamini-Hochberg multiple comparison adjustment via Metascape. All analyses utilized RNA purified from whole cell extracts of three biological replicates

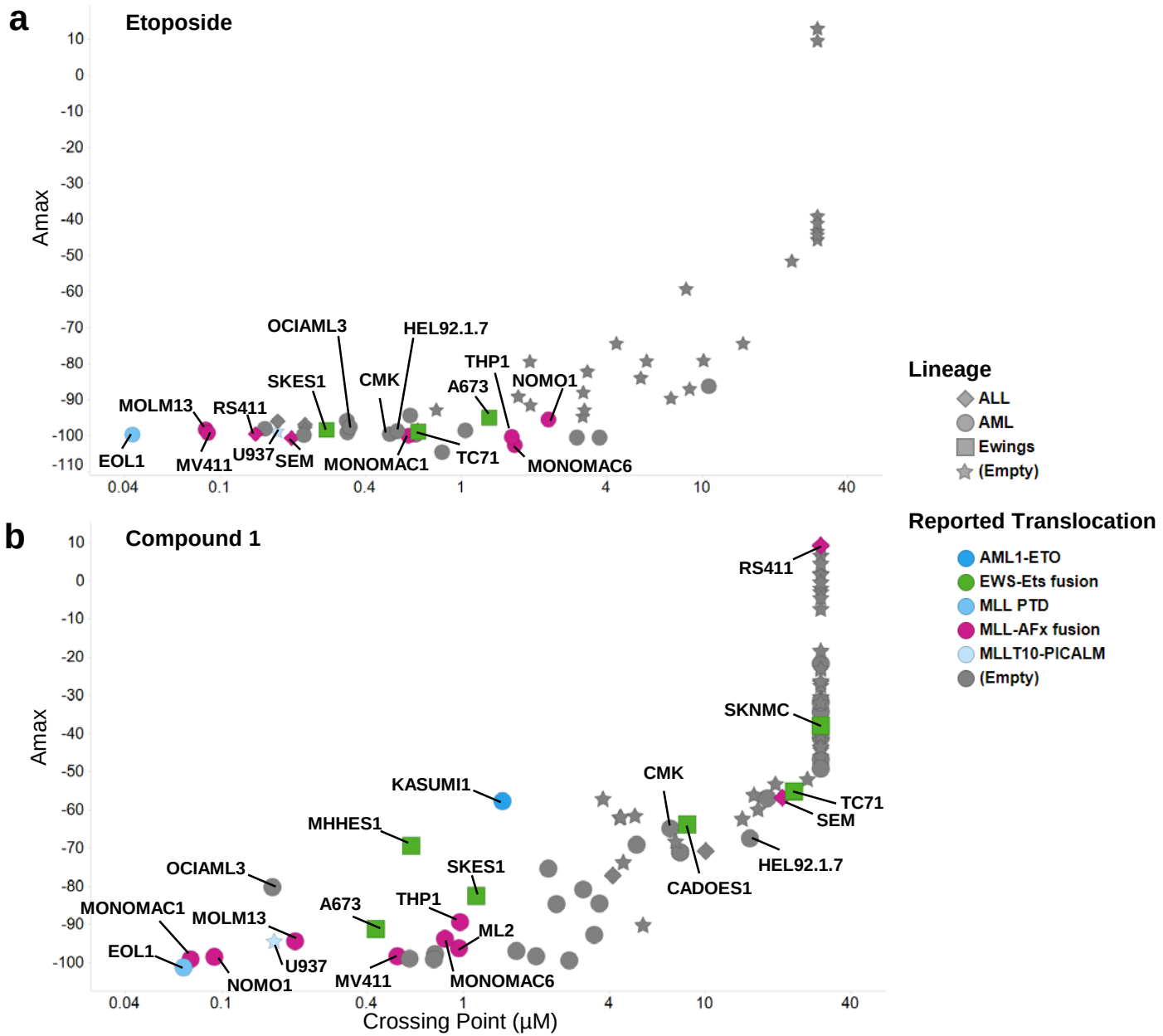

Supplementary Figure 19: **a**,**b**, Cell viability profile for (**a**) etoposide, analogous to experiment shown in Figure 1b for compound **1** and replotted here as (**b**). Note, the etoposide cell line panel was overlapping but did not include all 92 lines tested for compound **1**. Cell lines are shape-coded by lineage and color-coded by reported translocation. Lineage is given as ALL, AML, Ewing's or Other (Empty). Note: EWS-FLI translocated Ewing's lines TC71 and SKNMC have low CES1 expression.

MOLM-13 α-cMYC

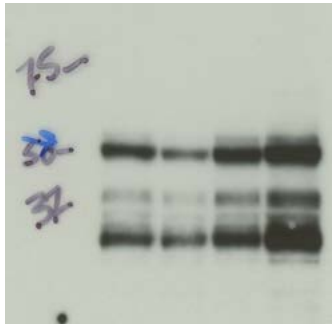

MOLM-13 α-cMYB

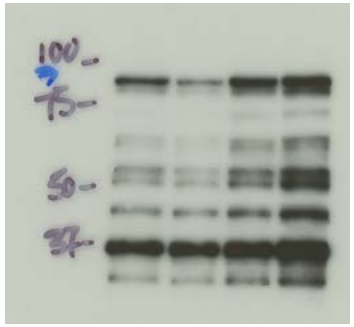

NOMO-1 α-cMYC

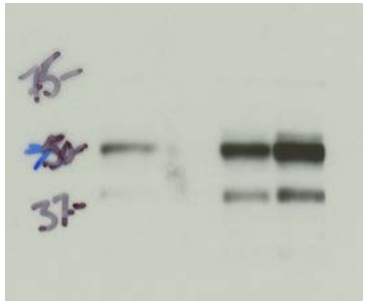

NOMO-1 α-cMYB

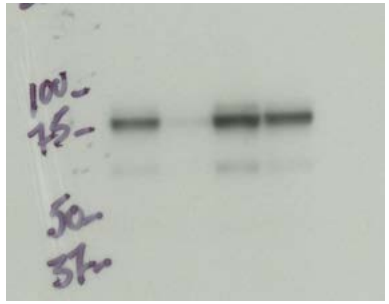

HEL 92.1.7 α-cMYB

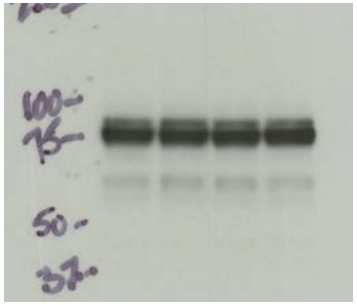

HEL92.1.7 α-cMYC

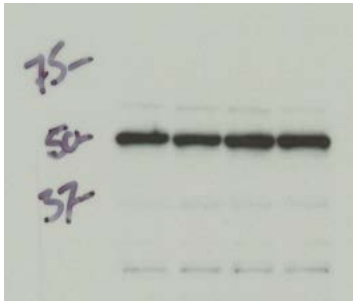

MOLM-13, Nomo-1, HEL 92.1.7, all with α-β-ACTIN

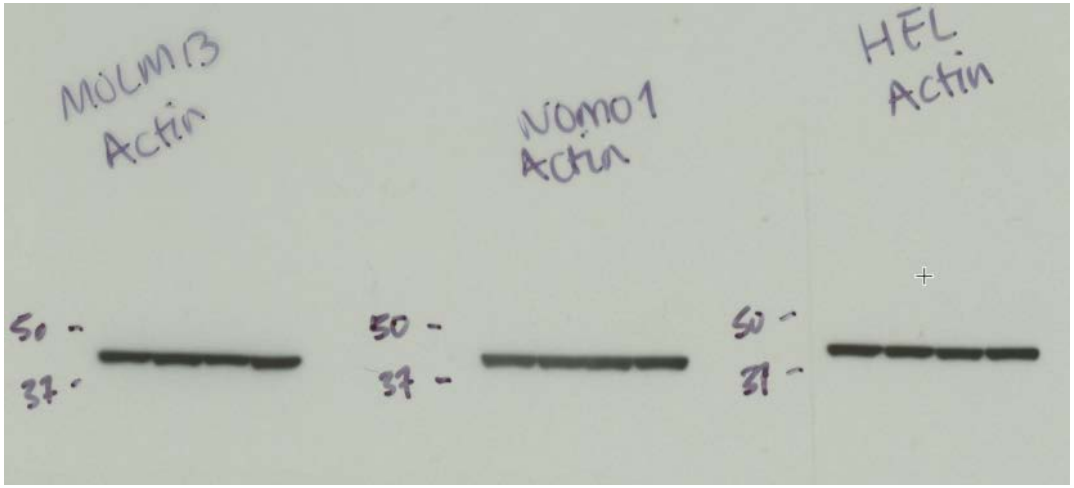

Supplementary Figure 20: Uncropped western blots for Supplementary Figure 2c. Sample order for all blots: Compound **1** 1μM, Compound **1** 10μM, Compound **3** 10μM; DMSO

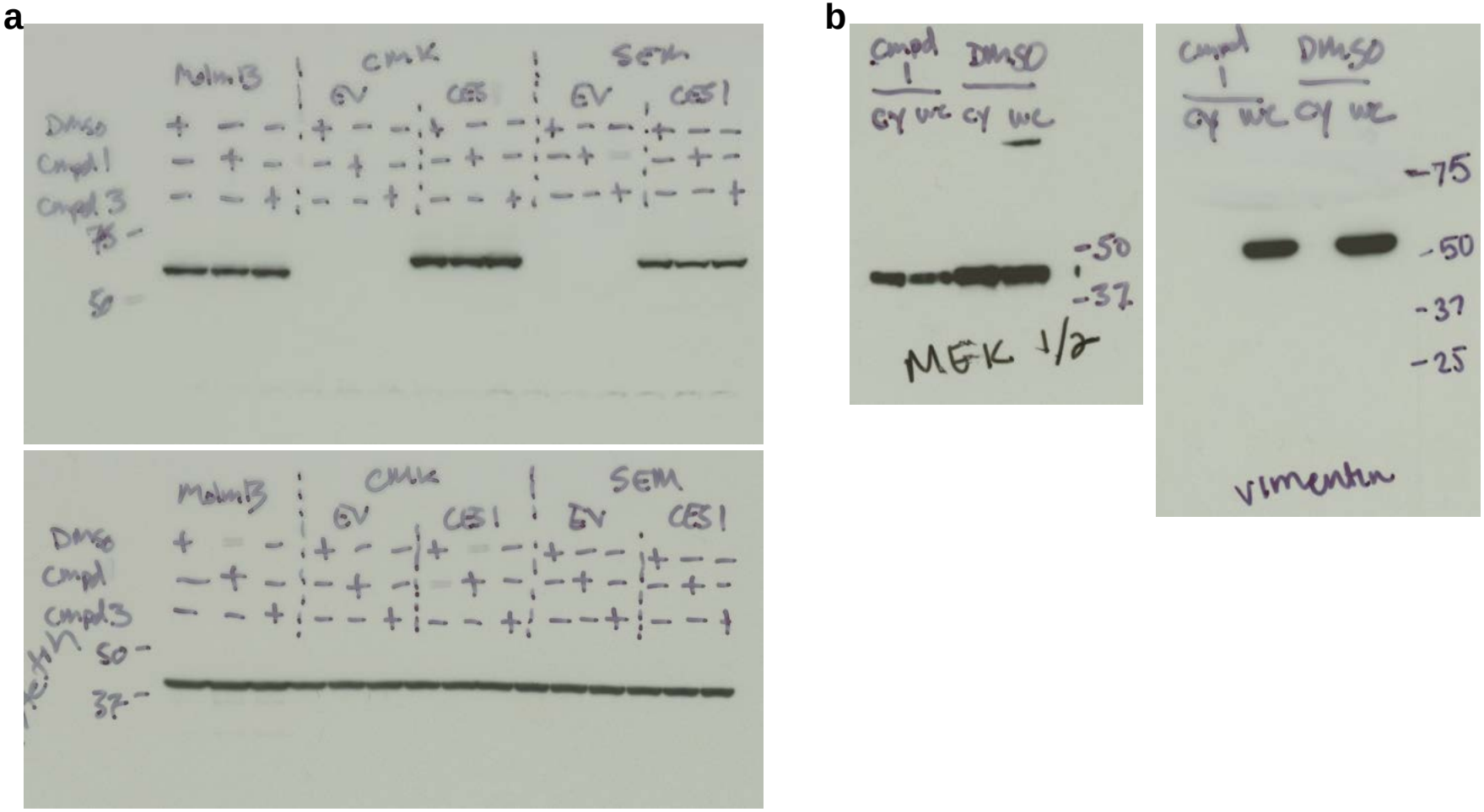

Supplementary Figure 21: **a**, Uncropped western blots for Supplementary Figure 8a (top: anti-CES1; bottom: anti-β-ACTIN). **b**, uncropped western blot for Supplementary Figure 16b (right: anti-MEK1/2; left: anti-VIMENTIN)

List of Supplementary Tables:

Supplementary Table 1: Panel of 92 cancer cell lines used in this study.

Supplementary Table 2: X-ray data collection and refinement statistics.

Supplementary Table 3: Antibodies used in this study.

Supplementary Table 4: smFISH probes used in this study.

Supplementary Notes

Supplementary Note- Synthetic Procedures: Chemical Synthesis Materials, General Spectroscopic Methods and Preparation of Compounds & Proton and Carbon NMR spectra compound 2, 3, 4, 5 and 7

List of Supplementary Data Sets provided as individual Excel files

Supplementary Data Set 1: siRNA library.

Supplementary Data Set 2: siRNA plus cmpd 1 synergy screen gene level activity per compound 1, or DMSO, or differential.

Supplementary Data Set 3: Chemoproteomics data.

Supplementary Data Set 4: PAL data.

Sorted_most(1)_to_least(92)_cmpd-sensitive	Cell_Line_Name	Primary_Site	Histology	Histology_Subtype	Clean_Name	Category	Translocation_Fusion_status	Cell Viability CTG assay IC50 range	CES1_expression_RNA-seq
1	MONO-MAC-1	haematopoietic_and_lymphoid_tissue	haematopoietic_neoplasm	acute_myeloid_leukaemia	monomac1	AML	KMT2A-MLLT3 (MLL-AF9)	sensitive: 0 < IC50 < 10 µM	high
2	EOL-1	haematopoietic_and_lymphoid_tissue	haematopoietic_neoplasm	acute_myeloid_leukaemia	eol1	AML	MLL partial tandem duplication	sensitive: 0 < IC50 < 10 µM	intermediate
3	U-937	haematopoietic_and_lymphoid_tissue	lymphoid_neoplasm	diffuse_large_B_cell_lymphoma	u937		MLLT10-PICALM	sensitive: 0 < IC50 < 10 µM	high
4	OCI-AML3	haematopoietic_and_lymphoid_tissue	haematopoietic_neoplasm	acute_myeloid_leukaemia	ociaml3	AML		sensitive: 0 < IC50 < 10 µM	high
5	MOLM-13	haematopoietic_and_lymphoid_tissue	haematopoietic_neoplasm	acute_myeloid_leukaemia	molm13	AML	KMT2A-MLLT3 (MLL-AF9)	sensitive: 0 < IC50 < 10 µM	high
6	NOMO-1	haematopoietic_and_lymphoid_tissue	haematopoietic_neoplasm	acute_myeloid_leukaemia	nomo1	AML	KMT2A-MLLT3 (MLL-AF9)	sensitive: 0 < IC50 < 10 µM	high
7	SKM-1	haematopoietic_and_lymphoid_tissue	haematopoietic_neoplasm	acute_myeloid_leukaemia	skm1	AML		sensitive: 0 < IC50 < 10 µM	intermediate
8	MHH-ES-1	bone	Ewings_sarcoma-peripheral_primitive_neuroectodermal_tumour	NS	mhhes1	Ewings	EWSR1-FLI1	sensitive: 0 < IC50 < 10 µM	high
9	A-673	bone	Ewings_sarcoma-peripheral_primitive_neuroectodermal_tumour	NS	a673	Ewings	EWSR1-FLI1	sensitive: 0 < IC50 < 10 µM	high
10	MONO-MAC-6	haematopoietic_and_lymphoid_tissue	haematopoietic_neoplasm	acute_myeloid_leukaemia	monomac6	AML	KMT2A-MLLT3 (MLL-AF9)	sensitive: 0 < IC50 < 10 µM	intermediate
11	MV-4-11	haematopoietic_and_lymphoid_tissue	haematopoietic_neoplasm	acute_myeloid_leukaemia	mv411	AML	KMT2A-AFF1 (MLL-AF4)	sensitive: 0 < IC50 < 10 µM	intermediate
12	ML-2	haematopoietic_and_lymphoid_tissue	haematopoietic_neoplasm	acute_myeloid_leukaemia	ml2	AML	KMT2A-MLLT4 (MLL-AF6)	sensitive: 0 < IC50 < 10 µM	
13	OCI-AML2	haematopoietic_and_lymphoid_tissue	haematopoietic_neoplasm	acute_myeloid_leukaemia	ociaml2	AML		sensitive: 0 < IC50 < 10 µM	high
14	NB-4	haematopoietic_and_lymphoid_tissue	haematopoietic_neoplasm	acute_myeloid_leukaemia	nb4	AML	PML-RARA	sensitive: 0 < IC50 < 10 µM	intermediate
15	SK-ES-1	bone	Ewings_sarcoma-peripheral_primitive_neuroectodermal_tumour	NS	skes1	Ewings	EWSR1-FLI1	sensitive: 0 < IC50 < 10 µM	high
16	THP-1	haematopoietic_and_lymphoid_tissue	haematopoietic_neoplasm	acute_myeloid_leukaemia	thp1	AML	KMT2A-MLLT3 (MLL-AF9)	sensitive: 0 < IC50 < 10 µM	high
17	WSU-AML	haematopoietic_and_lymphoid_tissue	haematopoietic_neoplasm	acute_myeloid_leukaemia	wsuaml	AML		sensitive: 0 < IC50 < 10 µM	
18	KBM-7	haematopoietic_and_lymphoid_tissue	haematopoietic_neoplasm	acute_myeloid_leukaemia	kbm7	AML		sensitive: 0 < IC50 < 10 µM	
19	PL-21	haematopoietic_and_lymphoid_tissue	haematopoietic_neoplasm	acute_myeloid_leukaemia	pl21	AML		sensitive: 0 < IC50 < 10 µM	high
20	AML-193	haematopoietic_and_lymphoid_tissue	haematopoietic_neoplasm	acute_myeloid_leukaemia	aml193	AML		sensitive: 0 < IC50 < 10 µM	low
21	HL-60	haematopoietic_and_lymphoid_tissue	haematopoietic_neoplasm	acute_myeloid_leukaemia	hl60	AML		sensitive: 0 < IC50 < 10 µM	intermediate
22	KASUMI-1	haematopoietic_and_lymphoid_tissue	haematopoietic_neoplasm	acute_myeloid_leukaemia	kasumi1	AML	RUNX1-RUNX1T1 (AML1-ETO)	sensitive: 0 < IC50 < 10 µM	low
23	SNU-878	liver	carcinoma	hepatocellular_carcinoma	snu878			sensitive: 0 < IC50 < 10 µM	high
24	BEN	lung	carcinoma	NS	ben			sensitive: 0 < IC50 < 10 µM	high
25	OCI-LY3	haematopoietic_and_lymphoid_tissue	lymphoid_neoplasm	diffuse_large_B_cell_lymphoma	ocily3			sensitive: 0 < IC50 < 10 µM	low
26	BC-3C	urinary_tract	carcinoma	transitional_cell_carcinoma	bc3c			sensitive: 0 < IC50 < 10 µM	high
27	P31/FUJ	haematopoietic_and_lymphoid_tissue	haematopoietic_neoplasm	acute_myeloid_leukaemia	p31fuj	AML		sensitive: 0 < IC50 < 10 µM	high
28	CMK-11-5	haematopoietic_and_lymphoid_tissue	haematopoietic_neoplasm	acute_myeloid_leukaemia	cmk115	AML		sensitive: 0 < IC50 < 10 µM	
29	MOLM-16	haematopoietic_and_lymphoid_tissue	haematopoietic_neoplasm	acute_myeloid_leukaemia	molm16	AML		sensitive: 0 < IC50 < 10 µM	intermediate
30	MOLT-16	haematopoietic_and_lymphoid_tissue	lymphoid_neoplasm	acute_lymphoblastic_T_cell_leukaemia	molt16	ALL		sensitive: 0 < IC50 < 10 µM	low
31	KO52	haematopoietic_and_lymphoid_tissue	haematopoietic_neoplasm	acute_myeloid_leukaemia	ko52	AML		sensitive: 0 < IC50 < 10 µM	low
32	Hep G2	liver	carcinoma	hepatocellular_carcinoma	hepg2			sensitive: 0 < IC50 < 10 µM	high
33	GSS	stomach	carcinoma	adenocarcinoma	gss			sensitive: 0 < IC50 < 10 µM	high
34	BDCM	haematopoietic_and_lymphoid_tissue	lymphoid_neoplasm	acute_lymphoblastic_B_cell_leukaemia	bdcm	ALL		intermediate: 10 < IC50 < 20 µM	low
35	huH-1	liver	carcinoma	hepatocellular_carcinoma	huh1			intermediate: 10 < IC50 < 20 µM	high
36	OCI-AML5	haematopoietic_and_lymphoid_tissue	haematopoietic_neoplasm	acute_myeloid_leukaemia	ociaml5	AML		intermediate: 10 < IC50 < 20 µM	low
37	CADO-ES1	bone	Ewings_sarcoma-peripheral_primitive_neuroectodermal_tumour	NS	cadoes1	Ewings	EWSR1-ERG	intermediate: 10 < IC50 < 20 µM	low
38	HuH-6	liver	other	hepatoblastoma	huh6			intermediate: 10 < IC50 < 20 µM	high
39	JHH-5	liver	carcinoma	hepatocellular_carcinoma	jhh5			intermediate: 10 < IC50 < 20 µM	high
40	GDM-1	haematopoietic_and_lymphoid_tissue	haematopoietic_neoplasm	acute_myeloid_leukaemia	gdm1	AML		intermediate: 10 < IC50 < 20 µM	low
41	SYO-1	soft_tissue	synovial_sarcoma	biphasic	syo1			intermediate: 10 < IC50 < 20 µM	low
42	CFPAC-1	pancreas	carcinoma	ductal_carcinoma	cfpac1			intermediate: 10 < IC50 < 20 µM	low
43	OCI-M1	haematopoietic_and_lymphoid_tissue	haematopoietic_neoplasm	acute_myeloid_leukaemia	ocim1	AML		intermediate: 10 < IC50 < 20 µM	low
44	CMK-86	haematopoietic_and_lymphoid_tissue	haematopoietic_neoplasm	acute_myeloid_leukaemia	cmk86	AML		intermediate: 10 < IC50 < 20 µM	
45	CMK	haematopoietic_and_lymphoid_tissue	haematopoietic_neoplasm	acute_myeloid_leukaemia	cmk	AML		intermediate: 10 < IC50 < 20 µM	low
46	NCI-H2172	lung	carcinoma	non_small_cell_carcinoma	ncih2172			intermediate: 10 < IC50 < 20 µM	high
47	QGP-1	pancreas	carcinoma	NS	qgp1			intermediate: 10 < IC50 < 20 µM	low
48	M-07e	haematopoietic_and_lymphoid_tissue	haematopoietic_neoplasm	acute_myeloid_leukaemia	m07e	AML		intermediate: 10 < IC50 < 20 µM	low
49	HCC-1588	lung	carcinoma	squamous_cell_carcinoma	hcc1588			intermediate: 10 < IC50 < 20 µM	low
50	JHOM-1	ovary	carcinoma	adenocarcinoma	jhom1			insensitive: IC50 > 20 µM	high
51	NCI-H520	lung	carcinoma	squamous_cell_carcinoma	ncih520			insensitive: IC50 > 20 µM	high
52	RMUG-S	ovary	carcinoma	adenocarcinoma	rmugs			insensitive: IC50 > 20 µM	high
53	SK-N-MC	bone	Ewings_sarcoma-peripheral_primitive_neuroectodermal_tumour	NS	sknmc	Ewings	EWSR1-FLI1	insensitive: IC50 > 20 µM	low
54	COLO-320	large_intestine	carcinoma	adenocarcinoma	colo320			insensitive: IC50 > 20 µM	low
55	SEM	haematopoietic_and_lymphoid_tissue	lymphoid_neoplasm	acute_lymphoblastic_B_cell_leukaemia	sem	ALL	KMT2A-AFF1 (MLL-AF4)	insensitive: IC50 > 20 µM	low
56	HEL 92.1.7	haematopoietic_and_lymphoid_tissue	haematopoietic_neoplasm	acute_myeloid_leukaemia	hel9217	AML		insensitive: IC50 > 20 µM	low
57	RS4;11	haematopoietic_and_lymphoid_tissue	lymphoid_neoplasm	acute_lymphoblastic_B_cell_leukaemia	rs411	ALL	KMT2A-AFF1 (MLL-AF4)	insensitive: IC50 > 20 µM	low
58	TC-71	bone	Ewings_sarcoma-peripheral_primitive_neuroectodermal_tumour	NS	tc71	Ewings	EWSR1-FLI1	insensitive: IC50 > 20 µM	low
59	COLO 205	large_intestine	carcinoma	adenocarcinoma	colo205			insensitive: IC50 > 20 µM	
60	MM603	skin	malignant_melanoma	NS	mm603			insensitive: IC50 > 20 µM	low
61	HCT 116	large_intestine	carcinoma	NS	hct116			insensitive: IC50 > 20 µM	low
62	VM-CUB1	urinary_tract	carcinoma	transitional_cell_carcinoma	vmcub1			insensitive: IC50 > 20 µM	low
63	SW 1353	bone	chondrosarcoma	NS	sw1353			insensitive: IC50 > 20 µM	intermediate
64	TF-1	haematopoietic_and_lymphoid_tissue	haematopoietic_neoplasm	acute_myeloid_leukaemia	tf1	AML		insensitive: IC50 > 20 µM	low
65	KMS-11	haematopoietic_and_lymphoid_tissue	lymphoid_neoplasm	plasma_cell_myeloma	kms11			insensitive: IC50 > 20 µM	low
66	SW982	soft_tissue	synovial_sarcoma	NS	sw982			insensitive: IC50 > 20 µM	low
67	MM473	skin	malignant_melanoma	NS	mm473			insensitive: IC50 > 20 µM	intermediate
68	MM138	skin	malignant_melanoma	NS	mm138			insensitive: IC50 > 20 µM	low
69	LI-7	liver	carcinoma	hepatocellular_carcinoma	li7			insensitive: IC50 > 20 µM	high
70	NCI-H1573	lung	carcinoma	adenocarcinoma	ncih1573			insensitive: IC50 > 20 µM	high
71	HuH-7	liver	carcinoma	hepatocellular_carcinoma	huh7			insensitive: IC50 > 20 µM	low
72	NCI-H661	lung	carcinoma	large_cell_carcinoma	ncih661			insensitive: IC50 > 20 µM	low
73	BFTC-909	kidney	carcinoma	NS	bftc909			insensitive: IC50 > 20 µM	intermediate
74	JIMT-1	breast	carcinoma	ductal_carcinoma	jimt1			insensitive: IC50 > 20 µM	low
75	KYSE-510	oesophagus	carcinoma	squamous_cell_carcinoma	kyse510			insensitive: IC50 > 20 µM	low
76	Hs 695T	skin	malignant_melanoma	NS	hs695t			insensitive: IC50 > 20 µM	low
77	Hs 936.T	skin	malignant_melanoma	NS	hs936t			insensitive: IC50 > 20 µM	low
78	KYSE-150	oesophagus	carcinoma	squamous_cell_carcinoma	kyse150			insensitive: IC50 > 20 µM	low
79	BICR 31	upper_aerodigestive_tract	carcinoma	squamous_cell_carcinoma	bicr31			insensitive: IC50 > 20 µM	low
80	LS1034	large_intestine	carcinoma	adenocarcinoma	ls1034			insensitive: IC50 > 20 µM	low
81	HCC1143	breast	carcinoma	ductal_carcinoma	hcc1143			insensitive: IC50 > 20 µM	low
82	BICR 18	upper_aerodigestive_tract	carcinoma	squamous_cell_carcinoma	bicr18			insensitive: IC50 > 20 µM	high
83	SNU-C4	large_intestine	carcinoma	adenocarcinoma	snuc4			insensitive: IC50 > 20 µM	low
84	NCI-H1373	lung	carcinoma	adenocarcinoma	ncih1373			insensitive: IC50 > 20 µM	low
85	OC 314	ovary	carcinoma	serous_carcinoma	oc314			insensitive: IC50 > 20 µM	low
86	SH-4	skin	malignant_melanoma	NS	sh4			insensitive: IC50 > 20 µM	low
87	CL-14	large_intestine	carcinoma	NS	cl14			insensitive: IC50 > 20 µM	intermediate
88	SNU-349	kidney	carcinoma	clear_cell_renal_cell_carcinoma	snu349			insensitive: IC50 > 20 µM	low
89	MM576	skin	malignant_melanoma	NS	mm576			insensitive: IC50 > 20 µM	intermediate
90	UKE1	haematopoietic_and_lymphoid_tissue	haematopoietic_neoplasm	acute_myeloid_leukaemia	uke1	AML		insensitive: IC50 > 20 µM	
91	Kasumi3	haematopoietic_and_lymphoid_tissue	haematopoietic_neoplasm	acute_myeloid_leukaemia	kasumi3	AML		insensitive: IC50 > 20 µM	
92	SK-MEL-2	skin	malignant_melanoma	NS	skmel2			insensitive: IC50 > 20 µM	

Supplementary Table 1: Panel of 92 cancer cell lines used in this study.
Screened CCLE lines are annotated by cell line name, primary site and histology. For AML lines, MLL-translocation status is given where known, as is EWS-translocation status for Ewing's sarcoma cell lines.
Cell lines are grouped into sensitive, intermediate or insensitive to compound 1 based on IC50 values derived from 72 h treatment in dose-response in cell viability in vitro growth assay with CellTiter Glo read-out.
CES1 expression level given per cell line is based on RNA-seq profiling of CCLE. Cell lines are numbered by sensitivity to compound 1 from most sensitive (1) to least sensitive (92).

Supplementary Table 2 X-ray data collection and refinement statistics for CPSF3-compound **2** co-crystal structure

	CPSF3/compound **2** (pdb code: 6M8Q)
Data collection	
Space group	$P4_32_12$
Cell dimensions	
a, *b*, *c* (Å)	106.2, 106.2, 206.0
α, β, γ (°)	90, 90, 90
Resolution (Å)	2.49 – 90 (2.49 – 2.51)
R_{merge}	0.138 (1.27)
R_{pim}	0.056 (0.507)
$CC_{1/2}$	0.996 (0.652)
$I / \sigma I$	12.6 (2.2)
Completeness (%)	99.7 (99.7)
Redundancy	7.1 (7.1)
Refinement	
Resolution (Å)	2.49
No. reflections	41,852
R_{work} / R_{free}	0.175 / 0.221
No. atoms	
Protein	7,255
Ligand/ion	84
Water	495
B-factors	
Protein	51.7
Ligand/ion	50.5
Water	56.1
R.m.s. deviations	
Bond lengths (Å)	0.010
Bond angles (°)	1.18

Only one crystal was needed to obtain the structure. Highest-resolution shell is shown in parentheses.

Supplementary Table 3: Antibodies used in this study

Antibody (epitope)	Manufacturer	Catalog Number	Application	Lot Number	Dilution	Link to manufacturer's validation data
PE-conjugated CD11b	BioLegend	301306	FACS	B183220	5ul/1E6 cells	https://www.biolegend.com/en-us/products/pe-anti-human-cd11b-antibody-768
PE-conjugated CD44	BioLegend	338808	FACS	B189534	5ul/1E6 cells	https://www.biolegend.com/en-us/products/pe-anti-human-cd44-antibody-5745
PE-conjugated CD54	BioLegend	353106	FACS	B169127	5ul/1E6 cells	https://www.biolegend.com/en-us/products/pe-anti-human-cd54-antibody-7447
PE-conjugated CD73	BioLegend	344004	FACS	B189876	5ul/1E6 cells	https://www.biolegend.com/en-us/products/pe-anti-human-cd73-ecto-5-nucleotidase-antibody-6092
Alexa 568 goat anti mouse	ThermoFisher Scientific	A11031	R-loop staining	2026148	1:1000	https://www.thermofisher.com/antibody/product/Goat-anti-Mouse-IgG-H-L-Highly-Cross-Adsorbed-Secondary-Antibody-Polyclonal/A-11031
Alexa 647 goat anti rabbit	ThermoFisher Scientific	A21245	R-loop staining	2051068	1:1000	https://www.thermofisher.com/antibody/product/Goat-anti-Rabbit-IgG-H-L-Highly-Cross-Adsorbed-Secondary-Antibody-Polyclonal/A-21245
Nucleolin	Abcam	ab22758	R-loop staining	GR303746-3	1:1000	https://www.abcam.com/nucleolin-antibody-ab22758.html
DNA-RNA Hybrid clone S9.6	Millipore	MABE1095	R-loop staining	06131_4	1:200	http://www.merckmillipore.com/CH/de/product/Anti-DNA-RNA-Hybrid-Antibody-clone-S9.6,MM_NF-MABE1095
CPSF3	Abgent	AT1610a	WB	11175	1:1000	http://www.abgent.com/products/AT1610a-CPSF3-Antibody-monoclonal-M01
FLI1	Abcam	ab124791	WB	YH112404C	1:1000	https://www.abcam.com/fli1-antibody-epr4645-ab124791.html
MEK1/2	Cell Signaling Technologies	8727	WB	5	1:1000	https://www.cellsignal.com/products/primary-antibodies/mek1-2-d1a5-rabbit-mab/8727
MYB	Cell Signaling Technologies	12319	WB	1	1:1000	https://www.cellsignal.com/products/primary-antibodies/c-myb-d2r4y-rabbit-mab/12319
MYC	Cell Signaling Technologies	13987	WB	5	1:1000	https://www.cellsignal.com/products/primary-antibodies/c-myc-d3n8f-rabbit-mab/13987
NKX2.2	Abcam	ab187375	WB	GR299445-4	1:1000	https://www.abcam.com/nkx22-antibody-nx2294-ab187375.html
VIMENTIN	Cell Signaling Technologies	5741	WB	1	1:1000	https://www.cellsignal.com/products/primary-antibodies/vimentin-d21h3-xp-rabbit-mab/5741
BETA-ACTIN	Sigma	A5441	WB	127M4866V	1:10000	https://www.sigmaaldrich.com/catalog/product/sigma/a5441

Supplementary Table 4: smFISH probes used in this study.

FISH probe	Accession Number(s)	Sequence	Sequence Name	Three Modification	Three Lambda Max
NKX2-2 mRNA	NM_002509.3	tagtttctaactccaggagg	NKX2-2 mRNA_1	Quasar 570	550 nm
NKX2-2 mRNA	NM_002509.3	aaagcacgcggaaatggacg	NKX2-2 mRNA_2	Quasar 570	550 nm
NKX2-2 mRNA	NM_002509.3	ttgtagcttcacttggtcaa	NKX2-2 mRNA_3	Quasar 570	550 nm
NKX2-2 mRNA	NM_002509.3	ccccaaaatttatgtcgcaa	NKX2-2 mRNA_4	Quasar 570	550 nm
NKX2-2 mRNA	NM_002509.3	ttgtgttggtcagcgacatg	NKX2-2 mRNA_5	Quasar 570	550 nm
NKX2-2 mRNA	NM_002509.3	caggtctaagatgtccttga	NKX2-2 mRNA_6	Quasar 570	550 nm
NKX2-2 mRNA	NM_002509.3	tcgtagaaggggttcttcag	NKX2-2 mRNA_7	Quasar 570	550 nm
NKX2-2 mRNA	NM_002509.3	cttggagcttgagtcctgag	NKX2-2 mRNA_8	Quasar 570	550 nm
NKX2-2 mRNA	NM_002509.3	ttgtcattgtccggtgactc	NKX2-2 mRNA_9	Quasar 570	550 nm
NKX2-2 mRNA	NM_002509.3	ttggagaaaagcactcgccg	NKX2-2 mRNA_10	Quasar 570	550 nm
NKX2-2 mRNA	NM_002509.3	tggaaccagatcttgacctg	NKX2-2 mRNA_11	Quasar 570	550 nm
NKX2-2 mRNA	NM_002509.3	cttcatcttgtagcggtggt	NKX2-2 mRNA_12	Quasar 570	550 nm
NKX2-2 mRNA	NM_002509.3	tgagcgcgtgacatggtttg	NKX2-2 mRNA_13	Quasar 570	550 nm
NKX2-2 mRNA	NM_002509.3	ttgtactgcatgtgctgcag	NKX2-2 mRNA_14	Quasar 570	550 nm
NKX2-2 mRNA	NM_002509.3	tagtggagccgagagtcaac	NKX2-2 mRNA_15	Quasar 570	550 nm
NKX2-2 mRNA	NM_002509.3	aatctgccactccaaggaga	NKX2-2 mRNA_16	Quasar 570	550 nm
NKX2-2 mRNA	NM_002509.3	ctgtaaacacggcgtagagt	NKX2-2 mRNA_17	Quasar 570	550 nm
NKX2-2 mRNA	NM_002509.3	agaagcgaagctgcgcaaac	NKX2-2 mRNA_18	Quasar 570	550 nm
NKX2-2 mRNA	NM_002509.3	gacgacattaacgctgggac	NKX2-2 mRNA_19	Quasar 570	550 nm
NKX2-2 mRNA	NM_002509.3	ggtctttttctcgttttcaa	NKX2-2 mRNA_20	Quasar 570	550 nm
NKX2-2 mRNA	NM_002509.3	gctgacaatatcgctactca	NKX2-2 mRNA_21	Quasar 570	550 nm
NKX2-2 mRNA	NM_002509.3	cagaacgtttacatggccat	NKX2-2 mRNA_22	Quasar 570	550 nm
NKX2-2 mRNA	NM_002509.3	aaagcgaaatctgccaccag	NKX2-2 mRNA_23	Quasar 570	550 nm
NKX2-2 mRNA	NM_002509.3	tcaccaccgatatttacaac	NKX2-2 mRNA_24	Quasar 570	550 nm
NKX2-2 mRNA	NM_002509.3	cctgaaggtcattttggcaa	NKX2-2 mRNA_25	Quasar 570	550 nm
NKX2-2 mRNA	NM_002509.3	agaaaggagttggacccaga	NKX2-2 mRNA_26	Quasar 570	550 nm
NKX2-2 mRNA	NM_002509.3	aatagctgagctccaagttc	NKX2-2 mRNA_27	Quasar 570	550 nm
RUNX3_Var1_Var2	NM_001031680.2; NM_004350.2	cggagtagttctcgtcattg	RUNX3_Var1_Var2_1	Quasar 570	550 nm
RUNX3_Var1_Var2	NM_001031680.2; NM_004350.2	gaagcgaaggtcgttgaacc	RUNX3_Var1_Var2_2	Quasar 570	550 nm
RUNX3_Var1_Var2	NM_001031680.2; NM_004350.2	atggtcagggtgaaactctt	RUNX3_Var1_Var2_3	Quasar 570	550 nm
RUNX3_Var1_Var2	NM_001031680.2; NM_004350.2	tcggagaatgggttcagttc	RUNX3_Var1_Var2_4	Quasar 570	550 nm
RUNX3_Var1_Var2	NM_001031680.2; NM_004350.2	ggaaggagcggtcaaactgg	RUNX3_Var1_Var2_5	Quasar 570	550 nm
RUNX3_Var1_Var2	NM_001031680.2; NM_004350.2	catggagaactggtaggagc	RUNX3_Var1_Var2_6	Quasar 570	550 nm
RUNX3_Var1_Var2	NM_001031680.2; NM_004350.2	catcactggtcttgaaggtt	RUNX3_Var1_Var2_7	Quasar 570	550 nm
RUNX3_Var1_Var2	NM_001031680.2; NM_004350.2	taacctatgcctctgtacaa	RUNX3_Var1_Var2_8	Quasar 570	550 nm
RUNX3_Var1_Var2	NM_001031680.2; NM_004350.2	gaagtatgggatgagacggc	RUNX3_Var1_Var2_9	Quasar 570	550 nm
RUNX3_Var1_Var2	NM_001031680.2; NM_004350.2	catagctggagacagtgagg	RUNX3_Var1_Var2_10	Quasar 570	550 nm
RUNX3_Var1_Var2	NM_001031680.2; NM_004350.2	ctctctggaagagagatggc	RUNX3_Var1_Var2_11	Quasar 570	550 nm
RUNX3_Var1_Var2	NM_001031680.2; NM_004350.2	ccaacagttaggaacggagg	RUNX3_Var1_Var2_12	Quasar 570	550 nm
RUNX3_Var1_Var2	NM_001031680.2; NM_004350.2	tgatgccatagactcatctt	RUNX3_Var1_Var2_13	Quasar 570	550 nm
RUNX3_Var1_Var2	NM_001031680.2; NM_004350.2	tgctttcctgggtttaagaa	RUNX3_Var1_Var2_14	Quasar 570	550 nm
RUNX3_Var1_Var2	NM_001031680.2; NM_004350.2	ctggtaaagtgcatggagga	RUNX3_Var1_Var2_15	Quasar 570	550 nm
RUNX3_Var1_Var2	NM_001031680.2; NM_004350.2	gaacagagagtggatgcgtt	RUNX3_Var1_Var2_16	Quasar 570	550 nm
RUNX3_Var1_Var2	NM_001031680.2; NM_004350.2	aaaatgatccctcacctcaa	RUNX3_Var1_Var2_17	Quasar 570	550 nm
RUNX3_Var1_Var2	NM_001031680.2; NM_004350.2	cagggacattgatgtctgac	RUNX3_Var1_Var2_18	Quasar 570	550 nm

RUNX3_Var1_Var2	NM_001031680.2; NM_004350.2	tcgcaagatttggctggatc	RUNX3_Var1_Var2_19	Quasar 570	550 nm
RUNX3_Var1_Var2	NM_001031680.2; NM_004350.2	ctatttgctttcagagcaca	RUNX3_Var1_Var2_20	Quasar 570	550 nm
RUNX3_Var1_Var2	NM_001031680.2; NM_004350.2	tacctgtaagagaccttgtg	RUNX3_Var1_Var2_21	Quasar 570	550 nm
RUNX3_Var1_Var2	NM_001031680.2; NM_004350.2	gcggggatgttgcttataat	RUNX3_Var1_Var2_22	Quasar 570	550 nm
RUNX3_Var1_Var2	NM_001031680.2; NM_004350.2	tagccccttgagaaagtatt	RUNX3_Var1_Var2_23	Quasar 570	550 nm
RUNX3_Var1_Var2	NM_001031680.2; NM_004350.2	aattcaggggcaagacttca	RUNX3_Var1_Var2_24	Quasar 570	550 nm
RUNX3_Var1_Var2	NM_001031680.2; NM_004350.2	ctgatgtgagaatccatgca	RUNX3_Var1_Var2_25	Quasar 570	550 nm
RUNX3_Var1_Var2	NM_001031680.2; NM_004350.2	ttttctaagcctttctaggg	RUNX3_Var1_Var2_26	Quasar 570	550 nm
RUNX3_Var1_Var2	NM_001031680.2; NM_004350.2	gttaaaataccgcatgctgc	RUNX3_Var1_Var2_27	Quasar 570	550 nm
RUNX3_Var1_Var2	NM_001031680.2; NM_004350.2	agcattttgtagggcagatt	RUNX3_Var1_Var2_28	Quasar 570	550 nm
RUNX3_Var1_Var2	NM_001031680.2; NM_004350.2	gctctcacagagacaaccaa	RUNX3_Var1_Var2_29	Quasar 570	550 nm
RUNX3_Var1_Var2	NM_001031680.2; NM_004350.2	taggatcaccagaaggactg	RUNX3_Var1_Var2_30	Quasar 570	550 nm
RUNX3_Var1_Var2	NM_001031680.2; NM_004350.2	aagagaaaccgcagcaggag	RUNX3_Var1_Var2_31	Quasar 570	550 nm
RUNX3_Var1_Var2	NM_001031680.2; NM_004350.2	cagggagtcagcaactattt	RUNX3_Var1_Var2_32	Quasar 570	550 nm
RUNX3_Var1_Var2	NM_001031680.2; NM_004350.2	ctaagaaggcatggagaggc	RUNX3_Var1_Var2_33	Quasar 570	550 nm
RUNX3_Var1_Var2	NM_001031680.2; NM_004350.2	acaatggattcatagctgct	RUNX3_Var1_Var2_34	Quasar 570	550 nm
RUNX3_Var1_Var2	NM_001031680.2; NM_004350.2	ccagagaacaggagggaaga	RUNX3_Var1_Var2_35	Quasar 570	550 nm
RUNX3_Var1_Var2	NM_001031680.2; NM_004350.2	gggttagtaatctgggatga	RUNX3_Var1_Var2_36	Quasar 570	550 nm
RUNX3_Var1_Var2	NM_001031680.2; NM_004350.2	ttacagactcagtacggctg	RUNX3_Var1_Var2_37	Quasar 570	550 nm
RUNX3_Var1_Var2	NM_001031680.2; NM_004350.2	aaggacctacttttaccagc	RUNX3_Var1_Var2_38	Quasar 570	550 nm
RUNX3_Var1_Var2	NM_001031680.2; NM_004350.2	acaactttaacgcagccttg	RUNX3_Var1_Var2_39	Quasar 570	550 nm
RUNX3_Var1_Var2	NM_001031680.2; NM_004350.2	ttcctacatcagtgtgtttg	RUNX3_Var1_Var2_40	Quasar 570	550 nm
RUNX3_Var1_Var2	NM_001031680.2; NM_004350.2	caaaacgtcttcctttcctc	RUNX3_Var1_Var2_41	Quasar 570	550 nm
RUNX3_Var1_Var2	NM_001031680.2; NM_004350.2	caggctcacagtaacactat	RUNX3_Var1_Var2_42	Quasar 570	550 nm
RUNX3_Var1_Var2	NM_001031680.2; NM_004350.2	aaagattggtacccactact	RUNX3_Var1_Var2_43	Quasar 570	550 nm
RUNX3_Var1_Var2	NM_001031680.2; NM_004350.2	cacacctcagcatgacaata	RUNX3_Var1_Var2_44	Quasar 570	550 nm
RUNX3_Var1_Var2	NM_001031680.2; NM_004350.2	tacatcagatgagtgcagca	RUNX3_Var1_Var2_45	Quasar 570	550 nm
RUNX3_Var1_Var2	NM_001031680.2; NM_004350.2	atagtgcaaagcagtttcca	RUNX3_Var1_Var2_46	Quasar 570	550 nm
RUNX3_Var1_Var2	NM_001031680.2; NM_004350.2	tgtacaagcaagttgtgcgt	RUNX3_Var1_Var2_47	Quasar 570	550 nm
RUNX3_Var1_Var2	NM_001031680.2; NM_004350.2	ttccacacatctcagagtta	RUNX3_Var1_Var2_48	Quasar 570	550 nm